Molecular Neurodegeneration

RESEARCH ARTICLE

Open Access

Regulation of the hippocampal translatome by Apoer2-ICD release

Catherine R. Wasser[1,2†], Gordon C. Werthmann[1,2†], Eric M. Hall[1,2], Kristina Kuhbandner[1,2], Connie H. Wong[1,2], Murat S. Durakoglugil[1,2] and Joachim Herz[1,2,3,4*]

Abstract

Background ApoE4, the most significant genetic risk factor for late-onset Alzheimer's disease (AD), sequesters a pro-synaptogenic Reelin receptor, Apoer2, in the endosomal compartment and prevents its normal recycling. In the adult brain, Reelin potentiates excitatory synapses and thereby protects against amyloid-β toxicity. Recently, a gain-of-function mutation in Reelin that is protective against early-onset AD has been described. Alternative splicing of the Apoer2 intracellular domain (Apoer2-ICD) regulates Apoer2 signaling. Splicing of juxtamembraneous exon 16 alters the γ-secretase mediated release of the Apoer2-ICD as well as synapse number and LTP, and inclusion of exon 19 ameliorates behavioral deficits in an AD mouse model. The Apoer2-ICD has also been shown to alter transcription of synaptic genes. However, the role of Apoer2-ICD release upon transcriptional regulation and its role in AD pathogenesis is unknown.

Methods To assess *in vivo* mRNA-primed ribosomes specifically in hippocampi transduced with Apoer2-ICD splice variants, we crossed wild-type, cKO, and Apoer2 cleavage-resistant mice to a Cre-inducible translating ribosome affinity purification (TRAP) model. This allowed us to perform RNA-Seq on ribosome-loaded mRNA harvested specifically from hippocampal cells transduced with Apoer2-ICDs.

Results Across all conditions, we observed ~4,700 altered translating transcripts, several of which comprise key synaptic components such as extracellular matrix and focal adhesions with concomitant perturbation of critical signaling cascades, energy metabolism, translation, and apoptosis. We further demonstrated the ability of the Apoer2-ICD to rescue many of these altered transcripts, underscoring the importance of Apoer2 splicing in synaptic homeostasis. A variety of these altered genes have been implicated in AD, demonstrating how dysregulated Apoer2 splicing may contribute to neurodegeneration.

Conclusions Our findings demonstrate how alternative splicing of the APOE and Reelin receptor Apoer2 and release of the Apoer2-ICD regulates numerous translating transcripts in mouse hippocampi *in vivo*. These transcripts comprise a wide range of functions, and alterations in these transcripts suggest a mechanistic basis for the synaptic deficits seen in Apoer2 mutant mice and AD patients. Our findings, together with the recently reported AD-protective effects of a Reelin gain-of-function mutation in the presence of an early-onset AD mutation in Presenilin-1, implicate the Reelin/Apoer2 pathway as a target for AD therapeutics.

Keywords Apoer2, Alzheimer's TRAP-Seq, Synaptic homeostasis, Reelin, ApoE, Alternative splicing

†Catherine Wasser and Gordon C. Werthmann contributed equally to this work.

*Correspondence:
Joachim Herz
Joachim.Herz@utsouthwestern.edu
Full list of author information is available at the end of the article

Graphical Abstract

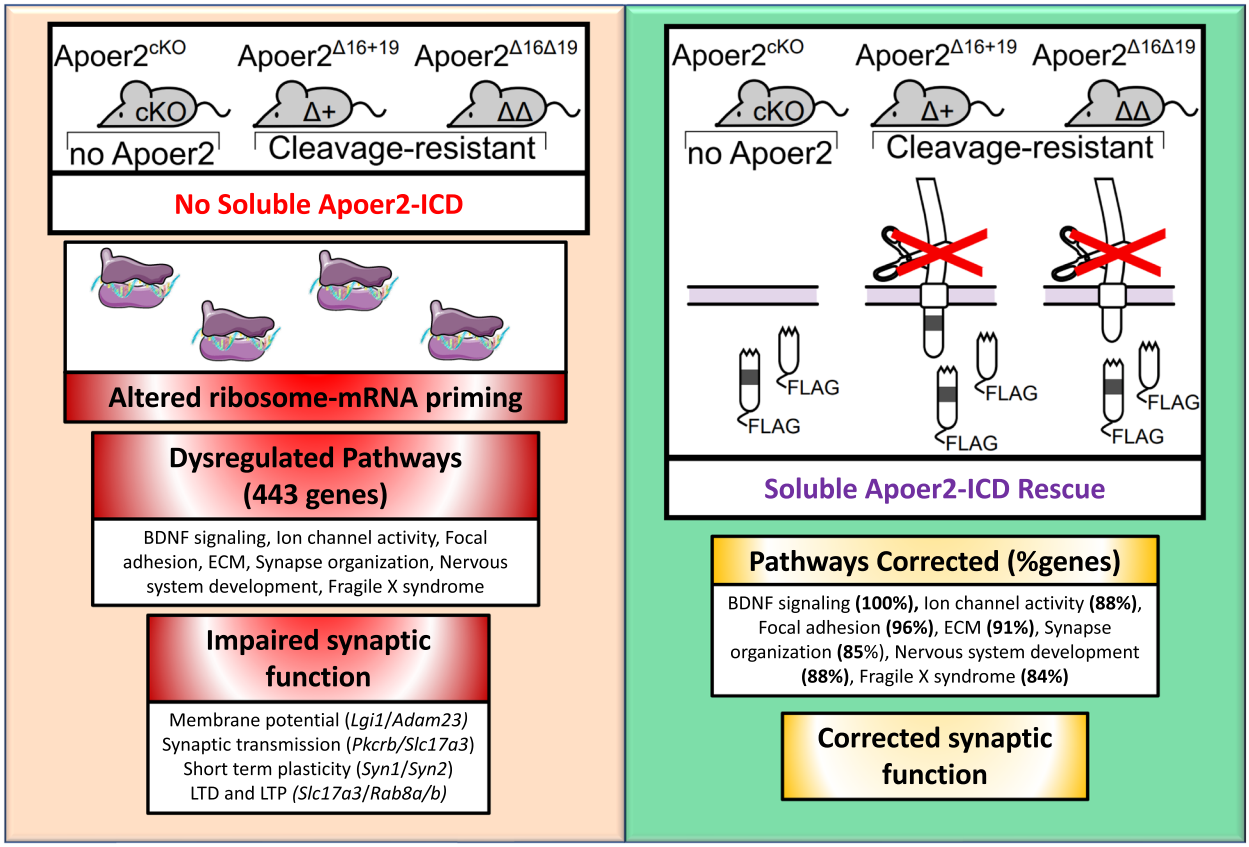

Background

Apolipoprotein E receptor 2 (Apoer2) and the very-low density lipoprotein receptor (Vldlr) are single-pass membrane proteins that act in concert with their ligand Reelin to orchestrate essential processes directing neurons to their final positions during development [30]. They are later repurposed as homeostatic regulators at the synapse where they are involved in synaptic formation, maturation, and strength [65, 69]. Apoer2 is expressed in various neuronal cell types including excitatory and inhibitory neurons in the hippocampus, cerebral cortex, cerebellum, and olfactory bulb as well as horizontal cells and bipolar cells in the retina [73], (Human Protein Atlas). Microglial cells, the resident immune cell of the brain, also express Apoer2. In humans, there are three isoforms of ApoE (ε2, ε3, ε4) which differ from each other by one or two amino acids. These coding polymorphisms are associated with a drastically different average age of onset of late-onset Alzheimer's disease (LOAD), whereby ApoE2 confers protection against and ApoE4 is the leading genetic risk factor for LOAD [17, 76].

The Apoer2 ligand, Reelin, is implicated in several neuropsychiatric and neurodegenerative diseases, such as autism, schizophrenia, bipolar disorder, major depression, and AD (reviewed in [8, 18, 21, 29, 47, 50, 51]). Functional Reelin expression is altered in AD [6, 12, 37], and its protective effects are antagonized by Aβ toxicity [51, 68]. Gene polymorphisms and altered splice variants of the ApoE/Reelin receptors, Apoer2 [36, 39, 82, 84], and Vldlr [82, 88] have been detected in AD patients. Most importantly, a gain-of-function mutation in Reelin has recently been reported to be protective against an aggressive, heritable form of early-onset AD [56]. The protective effect of Reelin gain-of-function mutations combined with the disease-associated effect of Apoer2 loss-of-function provides strong genetic evidence for this pathway at the core of AD pathophysiology.

How Apoer2 signaling regulates neuronal homeostasis is unknown. Alternative splicing of Apoer2 plays a critical role in synapse function and number [2, 26, 30, 65, 69, 70, 75, 78, 86], indicating a physiological need for functionally diverse forms of the receptor. Much like

other receptors (i.e. LRP1 and Notch), Apoer2 undergoes sequential cleavage [38, 60, 72, 91], releasing cleavage fragments on extracellular and intracellular sides of the membrane (Apoer2-ECD and -ICD, respectively). The Apoer2-ICD released by γ-secretase is reported to translocate to the nucleus and alter gene transcription similarly to the Lrp1-ICD [1, 48, 60, 61, 81, 93].

When splicing skips exon 16, Apoer2 lacks the O-linked sugar domain and is resistant to the initial proteolytic cleavage by extracellular metalloproteases, preventing the sequential release of the Apoer2-ECD and -ICD [86]. Mice expressing this cleavage-resistant Apoer2 (Apoer2$^{\Delta 16}$) in place of the endogenous receptor (Apoer2 knockin, KI) lack release of the Apoer2-ECD/ICD and have more Apoer2, more synapses, and reduced synaptic function [86]. A second alternatively spliced exon (19 in mice, 18 in humans) encodes a proline-rich cytosolic domain, which is differentially spliced in an activity-dependent manner [2, 74]. The inclusion of exon 19 is required for Reelin-mediated LTP enhancement through binding PSD-95 [2].

A human study of postmortem AD brains revealed increased exclusion of the proline-rich domain of Apoer2 [39]. The same splicing defect was observed in the brains of an AD mouse model, which have amyloid plaque deposition detectable at 3 months of age [39]. Delivery of antisense oligonucleotides that block exclusion of exon 19 prevented the cognitive deficits in this model [39]. While the role of this proline rich domain is unclear, exclusion of exon 19 in the cleavage-resistant Apoer2$^{\Delta 16}$ KI mice (Apoer2$^{\Delta 16\Delta 19}$) enhances the synaptogenic effect and further exacerbates the synaptic dysfunction compared to those with the proline-rich domain (Apoer2$^{\Delta 16+19}$). This suggests that inclusion of exon 19 can attenuate the loss of Apoer2 cleavage independent of transcriptional regulation which relies on cleavage of the Apoer2-ICD [81, 86].

To probe for the role of Apoer2-ICD splice variants, we sought to uncover whether the Apoer2-ICD is necessary and sufficient to regulate translation of key neuronal transcripts. This required a multi-model approach with three Apoer2 mouse lines – each lacking the presence (Apoer2^{cKO}) or release (Apoer2$^{\Delta 16+19}$ and Apoer2$^{\Delta 16\Delta 19}$) of the Apoer2-ICD and crossed to the Rosa26-TRAP (translating-ribosome affinity purification) mouse, which harbors a Cre-inducible GFP-tagged ribosomal subunit [34, 35]. Upon lentiviral delivery of Cre with or without the Apoer2-ICD[±19], we assessed the role of the Apoer2-ICD in regulating neuronal translating mRNA and the impact of alternative splicing on this regulation. Importantly, this method allowed us to isolate and sequence translating mRNA specifically from hippocampal cells *in vivo* which expressed exogenous soluble Apoer2-ICD, therefore ensuring changes to mRNA levels were specifically due to re-introduction of the Apoer2-ICD. When comparing our sequencing datasets to AD genetic risk loci, the ribosome association of 34 AD risk transcripts are differentially regulated. These findings are consistent with new genetic linkages with the Reelin signaling pathway in AD pathogenesis [7, 56], pointing to a likely underlying mechanism of Apoer2 and the Reelin signaling pathway in AD.

Methods

Experimental models and subject details

All mice were housed under a 12:12 light:dark cycle and fed a normal chow diet. All animals were euthanized by inhalation of isoflurane followed by decapitation according to strict regulations set by the National Institutes of Health Guide for the Care and Use of Laboratory Animals and the UT Southwestern Animal Care and Use Committee. All mice were maintained on a wild-type SV129 and C56BL/6J mixed background. The Apoer2$^{\Delta 16\pm 19}$ mouse lines have been previously described [86]. The conditional Apoer2 knockout was created by flanking exons 1 and 2 of the *Lrp8* gene with LoxP sites. TRAP mice expressing a GFP-tagged ribosomal subunit (L10a:GFP) after Cre-induced excision of an upstream floxed stop codon were purchased from Jackson Labs (Rosa26fsTRAP, Jax no: 022367).

Constructs

All sequences used are listed in Table S11. For the luciferase assay, 2.6-kb of the promoter regions of either human *Reln* or mouse *Lrp8* were cloned into the multiple cloning site of the Gaussia luciferase and secreted alkaline phosphatase reporter cloning vector (GeneCopoeia; pEZX-GA01; Cat#ZX103). The Apoer2-ICD expression plasmids were modified from [2] to include an N-terminal 3x-FLAG with or without a C-terminal VP16. For the TRAP constructs, the 3x-FLAG and Apoer2-ICD sequences were cloned into the pLVX-IRES-ZsGreen1 Vector (Clontech Cat#632187) and the ZsGreen sequence was replaced with the Cre-recombinase sequence.

Luciferase assay

HEK-293T or SH-SY5Y cells were co-transfected with dual reporter construct containing a CMV-driven secreted alkaline phosphatase (SEAP) and a Reelin promoter-driven secreted Gaussia luciferase (GLuc) reporter construct (GeneCopoeia, cat. no:pEZX-GA01) and either GFP or an Apoer2-ICD (Apoer2-ICD:VP16 construct (±exon 19, Apoer2-ICD[+19/Δ19]±VP16). After 24 hours, the media was collected from transfected cells and the luciferase and control SEAP intensity was quantified. Luciferase signal was normalized to the SEAP signal for

each well, then all values were normalized to media from cells transfected with an empty reporter construct and GFP (3-5 wells per condition, 2 parallel measurements, at least 2 independent experiments).

Lentiviral production

HEK-293T cells at 70-80% confluency in 10-cm plates were co-transfected with 3ug lentiviral construct, packaging, and envelope plasmids (ratio – 4:3:1) using Fugene6 transfection reagent following the manufacturers' instructions. Briefly, recombinant lentiviruses were produced by co-transfecting the cells with packaging (psPAX2; 2.25 μg) and the envelope vectors (pMD2.G; 0.75 μg) along with each lentiviral transfer vector (3 μg). Eight hours later, the cells were washed and fed with fresh culture medium containing 1mM sodium butyrate. The supernatant containing lentivirus particles was collected 48h after transfection followed by filtering through a 0.45μm filter and then concentrated to <100ul with a 10/30 kDa Amicon ultrafiltration filter. The concentrated lentivirus was layered over 10% sucrose (50mM Tris HCl pH 7.4, 100mM NaCl, 0.5mM EDTA, 10% sucrose) at a 4:1 ratio, then centrifuged at 14000 x g for 3 hours at 4°C. The subsequent pellet was resuspended in 1/100th of the original lentiviral media collected [43].

Lentivirus injection

Under continuous isoflurane anesthesia, 2-3 month old mice were stereotaxically injected (coordinates were AP: -2.2, ML: ±1.3, DV, -1.3) with concentrated lentivirus bilaterally to the CA1 hippocampal region with one of the three lentiviral constructs to express Cre only or both Cre and the Apoer2-ICD[±19] (empty-IRES-Cre and Apoer2-ICD[±19]-IRES-Cre). A total of 48 mice were injected (24 male, 24 female).

Translating ribosome affinity purification (TRAP)

Affinity matrix preparation

The matrix was prepared as described in [34]. For one hippocampus, the ratio of the components was 300ug Streptavidin MyOne T1 Dynabeads: 20μg biotinylated protein L: 50μg each of GFP antibodies 19C8 and 19F7 (100 μg total antibody). The appropriate amount of resuspended Dynabeads were washed once with 1X PBS (1:10 dilution of Phosphate-Buffered Saline (10X) from Invitrogen™ AM9625). Beads were then rotated end-over-end with biotinylated protein L in 1× PBS for 1 hour at room temperature and washed five times with 3% BSA (in 1X PBS). The protein L-conjugated beads were then rotated end-over-end for 1 hour with the GFP antibodies in a low-salt buffer (in RNase-free water: HEPES (pH 7.3), 20mM,KCl, 150mM; $MgCl_2$, 10mM; NP-40, 1%; add immediately before use: DTT, 0.5mM; cyclohexamide, 100μg/ml). Antibody-conjugated beads were not vortexed after this step. After washing three times with the low-salt buffer, the affinity matrix was aliquoted into tubes for individual hippocampal immunoprecipitations. Note: Before all bead washing steps, tubes were kept against the magnet for at least one minute before removing solutions to prevent loss of beads.

Tissue isolation and homogenization

Two months post-lentiviral injection, mice were anesthetized with isoflurane, quickly decapitated and the whole brain removed and placed on an ice-cold metal sheet. The brain was halved and placed into an icy slurry of cyclohexamide-containing dissection buffer (in RNase-free water: HEPES (pH 7.3), 2.5mM; HBSS, 1X; glucose, 35mM; $NaHCO_3$, 4mM; add immediately before use: cyclohexamide, 100ug/ml). Dissections were performed on the left hemisphere while keeping the other hemisphere in the slurry, the cerebellum and cortex were quickly dissected from the first hemisphere and snap frozen in liquid nitrogen. The hippocampus was immediately homogenized in tissue-lysis buffer (1mL/25-50mg) (in RNase-free water: HEPES (pH 7.3), 20mM; KCl, 150mM; $MgCl_2$, 10mM; add immediately before use: EDTA-free protease inhibitors , 1tab; DTT, 0.5mM; cyclohexamide, 100ug/ml; rRNasin, 10ul/ml; HEPES (pH 7.3), 20mM; SUPERase·In, 10ul/ml) with a 1-mL glass dounce homogenizer on ice followed by 10 strokes through a 23-gauge syringe. Lysates from the left hemisphere were incubated on ice while dissecting and homogenizing the right hippocampi. Lysates were centrifuged for 10 minutes at 2,000 x g at 4°C to remove nuclei (S2), and the supernatant was transferred to a fresh tube. A 1/9 volume of 10% NP-40 was added (1% final), followed by gentle inversion to mix and a brief pulse spin to prevent lysate loss. A 1/9 volume of 300mM DHPC (30mM final, prepared fresh each week in RNase-free water), followed by inversion to mix and incubated on ice for 5 minutes before centrifuging for 20 minutes at 20,000 x g at 4°C to remove mitochondria (S20). A small aliquot (~5%) was kept and stored at 4°C until after final RNA purification. The remaining supernatant was transferred to a fresh tube for immunopurification.

Immunopurification

The appropriate amount of freshly washed and resuspended affinity matrix (see Affinity matrix preparation section) was added to each lysate and incubated overnight (~18 hours) at 4°C with gentle end-over-end mixing. The next day, always keeping the tubes on ice, the beads were washed to reduce non-specific binding prior to RNA purification as described in [34]. Tubes were pulse-centrifuged and beads were allowed to collect for at

least one minute before each washing step. Briefly, tubes were quickly pulse-centrifuged then placed against the magnetic rack surrounded by ice. The GFP:L10-depleted lysate was removed and stored at -80°C. The beads bound to the RNA-GFP:L10 complexes were washed 4 times by resuspending beads by pipetting with 1mL of high-salt buffer (in RNase-free water: HEPES (pH 7.3), 20mM,KCl, 350mM; $MgCl_2$, 10mM; NP-40, 1%; add immediately before use: DTT, 0.5mM; cyclohexamide, 100ug/ml). Of note, during each wash, beads were pipetted at least 3 more times after visible resuspension and bubbles were avoided. After removing the fourth wash, beads were removed from the magnet and warmed to room temperature before RNA purification.

RNA purification

RNA was isolated from the GFP:L10-bound affinity matrix with the Absolutely RNA Nanoprep kit (Agilent, see Materials section) at room temperature. Briefly, 100µl of Nanoprep lysis buffer (with fresh ß-ME) was added to the beads. Tubes were vortexed and incubated for 10 minutes at room temperature. The tubes were then placed back on the magnet and the RNA-containing lysate was removed for purification according to the manufacturer's protocol with the following exception. Purified RNA was resuspended in 10uL of RNase-free water instead of the Elution buffer provided with the kit. IP RNA was aliquoted before freezing at -80°C. This elution buffer interfered with the accurate assessment of quality and approximate quantity of RNA by the 2100 Bioanalyzer with the Total RNA Pico chip (performed by the UTSW Genomics Sequencing Core). We obtained pico- to nanogram amounts of IP-RNA.

RNA amplification/ RNA-sequencing

RNA amplification

RNA amplification was performed as described in [63] with the exception that we used Superscript IV instead of Superscript III. aRNA concentration was estimated with the Agilent PicoChip before submitting aRNA for library preparation and RNA-sequencing. For RNA-sequencing, we needed a minimum of 50ng of RNA, as we wanted to sequence samples separately, we performed a pilot experiment where we amplified 100pg pooled IP RNA from a subset of our IP RNA. This pilot experiment confirmed that we could successfully sequence amplified IP RNA. We then amplified 100pg of our highest quality IP RNA from each genotype and then assessed the quality and rough concentration before submitting 48 amplified RNA samples for library preparation and RNA-sequencing (6-9 mice/genotype, with at least one male or female represented per condition). Libraries were prepared with the Illumina TruSeq Stranded mRNA kit and run on NextSeq sequencing SE-75 (all across 3 flow cells) by the UTSW Genomics Sequencing Core.

Bioinformatics

Reads were uploaded to the Galaxy online resource (https://usegalaxy.org/) and aligned to the mouse genome (mm10) using the STAR package (version 2.5.2b-0, [24]) with the ENCODE annotation (M21, ENCFF871VGR, [16, 59]). To remove 3'UTR bias in amplified RNA reads, the reads mapping to UTRs were filtered from the aligned BAM files. Gene counts were calculated by featureCounts (version 1.6.4+galaxy2), [54]. Differential gene expression was performed with the Deseq2 package (version 2.11.40.6+galaxy1), [58] to quantify the differential expression within genotypes with and without either Apoer2-ICD. Each condition was also tested against the $Apoer2^{WT}$ injected with the empty-IRES-Cre lentivirus. "Rescue" and "effect" *p*-values were calculated using an additive combining of *p*-value method, which is calculated by raising the sum of the *p*-values to the power of the number of *p*-values summed divided by the factorial of number of *p*-values summed [15]. The "rescue" *p*-values take into account the baseline effect of genotype compared to wildtype and the effect of the ICD in the genotype (i.e. *p*-value of $Apoer2^{cKO}$-cre vs $Apoer2^{WT}$-cre and $Apoer2^{cKO}$+ICDcre vs $Apoer2^{cKO}$-cre). Transcripts were considered rescued if: (1) rescue *p*-value <0.05, (2) a baseline |log2FC|>0.58 compared to WT, and (3) a log2FC compared to WT at least 0.5 closer to zero with the ICD±19 than without it. "Rescued" transcripts were also considered significant basal differences. The "effect" *p*-values take into account the effect of ICD compared to baseline genotype and wildtype (i.e. *p*-value of $Apoer2^{cKO}$+ICD vs $Apoer2^{WT}$-cre and $Apoer2^{cKO}$+ICDcre vs $Apoer2^{cKO}$-cre). Transcripts were considered effected if: (1) effect *p*-value <0.05 or rescue *p*-value <0.05 and (2) |log2FC|>0.58 with the ICD compared to both WT and baseline genotype. The exact *p*-values combined are noted in the column headers of Supplemental Table 10. The rescue and effect *p*-values were calculated for each ICD, and these *p*-values were further combined to calculate whether both ICDs significantly rescue or affect each transcript.

Significant basal differences of each genotype compared to $Apoer2^{WT}$ were defined as |log2FC|>0.58 and either a *p*-value <0.05, a "rescue" *p*-value <0.05, or a combined vWT *p*-value <0.05. When the log2FC compared to wildtype with and without the ICDs were both changed in the same direction (|log2FC|>0.58),

the "vWT" *p*-values were calculated by combining the *p*-values of wildtype control groups with and without the ICD (i.e. *p*-value of Apoer2^{cKO}-cre vs Apoer2^{WT}-cre and Apoer2^{cKO}+ICDcre vs Apoer2^{WT}-cre). Heatmaps were created with Morpheus (https://software.broadinstitute.org/morpheus/) and hierarchical clustering was performed with Euclidian distance using complete linkage. Supervenns were created with the Compare Sets Appyter [14]. Protein-protein interactions were created with STRING and Metascape [92]. These programs were also used to find functional enrichments along with ToppFun [11] and DAVID [20]. Gene families were identified with Gene Set Enrichment Analysis (GSEA) online (https://www.gsea-msigdb.org/gsea/msigdb/) [62, 77]. The core minimal network was comprised from the following enrichment categories: synapse organization (GO:0034329: cell junction assembly,GO:0034330: cell junction organization,GO:0050807, GO:0099175: regulation of synapse/postsynapse organization), neuron development (GO:0051960: regulation of nervous system development,GO:0048666: neuron development, GO:0048699: generation of neurons; GO:0022008: neurogenesis), focal adhesion (Wikipathway, WP306; KEGG, hsa04510; GO:0005925), extracellular matrix (ECM: GO:0030198, REACTOME, R-HSA-1474244), Fragile X Syndrome (Wikipathway, WP4549), BDNF signaling (Wikipathway, WP2380), and ion channel activity (GO:0005216) (Fig. 1F). Cell type approximation (Figure S6) was performed by comparing differentially expressed ribosome-associated transcripts to a previously published single-cell RNA-Seq hippocampal dataset [45].

Data analysis

Statistical analyses were performed with Graphpad Prism 8 software using one-way and two-way ANOVA with Tukey's *post hoc* multiple comparisons test for exact multiplicity adjusted *p*-values between groups. All data sets were checked for normality with the D'Agostino & Pearson omnibus or KS normality test. If data was non-normal, the non-parametric Kruskal-Wallis test was performed with Dunn's *post hoc* multiple comparisons test.

Results

Apoer2-ICD regulation of ribosome-associated transcripts *in vivo*

Apoer2 plays a critical role in synaptic function and number – both are regulated by alternative splicing [2, 26, 30, 65, 69, 75, 86]. This splicing regulates Apoer2 cleavage as well as synaptic plasticity and interactions [2, 70, 85, 86], however, the role of splicing in Apoer2-ICD-dependent transcript regulation is unknown. Mice expressing the cleavage-resistant Apoer2 (Apoer2$^{\Delta16}$) in place of the endogenous receptor (Apoer2 knockin, KI) lack release of the Apoer2-ECD/ICD and have more Apoer2 mRNA and protein, more synapses, and reduced synaptic function [86]. Exclusion of exon 19 in the cleavage-resistant Apoer2$^{\Delta16}$ KI mice (Apoer2$^{\Delta16\Delta19}$) further exacerbates the synaptic dysfunction and synaptogenesis resulting from the loss of Apoer2 cleavage (Apoer2$^{\Delta16}$), suggesting that the proline-rich domain does impart a synaptic effect independent of the release of the ICD [86].

To determine how the Apoer2-ICD release and its splicing regulate synapses, we crossed Rosa26-TRAP mice, which express a Cre-inducible GFP-tagged ribosomal subunit (L10a:GFP), to Apoer2 mutant mice which lack all or part of the Apoer2-ICD: a conditional Apoer2 knockout (Apoer2^{cKO}) and two cleavage-resistant Apoer2 lines (Apoer2$^{\Delta16}$) either with the proline-rich domain (Apoer2$^{\Delta16+19}$) or without it (Apoer2$^{\Delta16\Delta19}$) [34, 35] (Fig. 1A). We then delivered the Apoer2-ICD with or without exon 19 (Apoer2-ICD[±19]-IRES-Cre) to the hippocampi of these mice via lentiviral injection to demonstrate the sufficiency of the Apoer2-ICD to alter the expression of key synaptic transcripts in vivo (Fig. 1B, C). We next performed next generation RNA-Seq specifically on hippocampal cells infected with Cre-expressing lentivirus, allowing us to precisely identify transcripts affected by the Apoer2-ICD within the complex physiology of the living brain.

(See figure on next page.)

Fig. 1 Apoer2-ICD regulation of translating transcripts *in vivo*. **A** Rosa$^{26fs\text{-}TRAP}$ mice crossed with the Apoer2^{WT}, conditional KO, and cleavage-resistant Apoer2 transgenic mice (Apoer2$^{\Delta16\pm19}$) were injected with lentiviruses expressing Cre resulting in a GFP-tagged ribosomal subunit (L10a:GFP) to allow for pull-down of ribosome-bound transcripts (intrahippocampal injections; coordinates were AP: -2.2, ML: ±1.3, DV, -1.3). Using an Internal Ribosome Entry Site (IRES), Apoer2-ICD$^{[\pm19]}$ was co-expressed to assess the effect of overexpression of either Apoer2-ICD in Apoer2^{WT} or rescue of effects of lack of the Apoer2-ICD (**B**). **C**-**D** Heatmaps representing the proportion of genes altered in Apoer2 transgenic mice that are either rescued or not rescued with the Apoer2-ICD*[±19]* (**C**) or altered by overexpression of either Apoer2-ICD in Apoer2^{WT} or (**D**) effects of the ICD independent of the lack of ICD-release. **E** Enrichment analysis of the ~4700 transcripts differentially translated across all conditions, demonstrating enrichment for synaptic compartments, neuronal processes and pathways, as well as diseases of the brain. **F** Gene-term network of the ClueGO/Cluepedia enrichment analysis of synaptic transcripts annotated in the SynGO database. (For each mouse line: Cre-only and Cre+Apoer2-ICD[+19]: *n*= 4 individual and one pooled set of 4 RNA samples, Cre+Apoer2-ICD[Δ19]: *n*= 4 individual RNA samples)

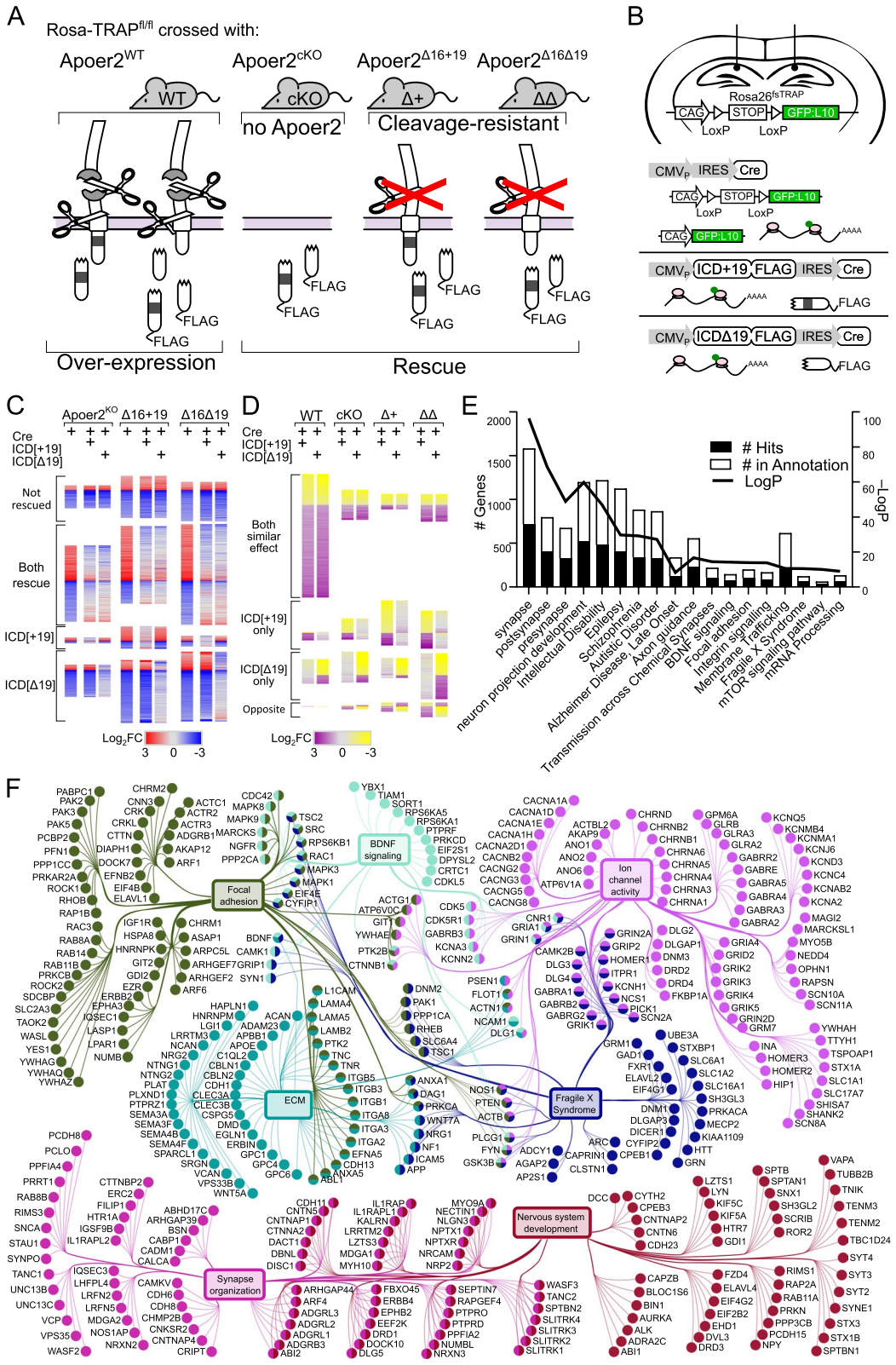

Fig. 1 (See legend on previous page.)

We utilized this rich RNA-Seq dataset to answer key questions regarding the function of Apoer2 splicing on hippocampal mRNA primed ribosomes. First, we compared the basal effect of the loss of nuclear Apoer2-ICD transcriptional regulation by comparing the ribosome-associated transcripts from the hippocampi of Apoer2 KI/cKO to the wild-type Apoer2 injected with lentivirus expressing only Cre. We then identified whether the Apoer2-ICD variants could rescue these effects. Afterwards, we looked for the effects imparted by the expression of either Apoer2-ICD variants independent of genotype. To ensure the difference between Apoer2-ICD with and without exon 19 was not due to the inability of Apoer2-ICD[Δ19] to act as a transcriptional regulator, we tested the binding of our Apoer2-ICD constructs to the *Reln* (a known Apoer2-ICD-regulated gene) promotor using a *Gaussia* luciferase reporter construct driven by 2.5 kb of the *Reln* promoter (see methods). As the cleavage-resistant Apoer2 mice have elevated Apoer2 transcription and translation, we also evaluated whether these Apoer2-ICD splice variants bind the promoter of Apoer2 (*Lrp8* promoter) (Figure S1A-C). We found no difference between the effects of Apoer2-ICD[+19] and Apoer2-ICD[Δ19] on luciferase expression controlled by *Reln* and *Lrp8* promoters (Figure S1D-G). This suggests that the Apoer2-ICD can regulate the transcription of at least a subset of its target genes independent of exon 19.

Across all conditions, the ribosome association of ~4,700 transcripts were altered (Fig. 1 C, D, Table S1-4). Approximately half of the altered transcripts were basal differences between the Apoer2 cKO/KI and the wild-type when injected with lentivirus expressing only Cre (Fig. 1C, Figure S2A). In addition, the majority of translating mRNAs were restored when Apoer2-ICD[±19]-IRES-Cre was injected and a smaller portion were either not rescued or rescued by only one of the Apoer2-ICD splice variants (Fig. 1C). The other half of the overall altered transcripts were a result of genotype-independent effects of lentiviral expression of the Apoer2-ICD in the wild-type or Apoer2 cKO/KI mice (Fig. 1D). We found that in the Apoer2^{WT}, the majority of transcripts are similarly regulated by both Apoer2-ICD splice variants, with a smaller portion regulated by only one of the Apoer2-ICD splice variants; however, across the Apoer2 cKO/KI mice the effects of the Apoer2-ICD variants are more diverse (Fig. 1D).

The overall dataset was highly enriched for synaptic compartments and neuronal processes/pathways as well as diseases of the brain by ToppFun enrichment analysis (https://toppgene.cchmc.org/enrichment.jsp) [11] (Fig. 1E). To further elucidate the effect of the Apoer2-ICD on synaptic gene regulation, we identified specific transcripts with known synaptic localization and/or function using the SynGo database [49] which contains manual curations from numerous published studies. Of the 4,658 altered transcripts, 610 were annotated in the database with synaptic localization and/or function. We focused on those 610 synaptic genes and created a functional enrichment network using the ClueGO [5] with Cluepedia [4] applications in the Cytoscape App [57]. This workflow linked ~443 of these synaptic genes to six core clusters: synapse organization, neuron development, focal adhesion, extracellular matrix (ECM), Fragile X Syndrome, BDNF signaling, and ion channel activity (Fig. 1F). In addition, we have also manually gathered all the transcripts annotated under these categories and expanded the network to include those not annotated in the SynGo database, resulting in a total of 1,301 transcripts. The residual 208 SynGO synaptic transcripts not included in the minimal synaptic network in Fig. 1F are enriched for neurotransmitter transport, synaptic transmission, synaptic vesicle cycle and membrane trafficking. The 3,146 non-SynGO transcripts not included in the minimal Apoer2-ICD network were enriched for mRNA processing as well as oxidoreductase activity, chromatin modification, cell cycle and metabolism of lipids.

Basal ribosome loaded mRNA differences in Apoer2^{cKO} and cleavage-deficient Apoer2$^{\Delta 16}$ mutant hippocampus

When we compared the transcripts affected by complete loss of the protein (Apoer2^{cKO} with IRES-Cre) or lack of the release of the ICD (Apoer2$^{\Delta 16\pm 19}$ with IRES-Cre), there were a total of 2,953 differentially regulated translating transcripts across all Apoer2 KI/cKO genotypes compared to Apoer2^{WT} (Figs. 1C, 2A, S3A, Figure S2B, C Table S2-4); however, only 125 (4%) of these are significantly altered in all three Apoer2^{cKO} and cleavage-deficient genotypes (Figs. 1C, 2A, B), which outlines the effects of the Apoer2-ICD on ribosomal mRNA loading. Half of these transcripts were either SynGO or known disease-associated transcripts. Of these, there are 16 up-regulated transcripts with 4 involved in the PI3K-AKT signaling pathway (COL1A2, RPTOR, LAMA4, TNC), and 92 down-regulated transcripts with 5 known to modulate neurotransmission (ARC, ARHGAP44, CDKL5, TNR, TUBB2B) and 6 involved in the synaptic vesicle cycle (PPFIA2, ABI1, AP1G1, PRKCB, RAB3B, SCRN1). Of the transcripts significantly altered in all three genotypes in opposing directions, 11 transcripts were similarly regulated in the Apoer2^{cKO} and Apoer2 $^{\Delta 16\Delta 19}$ with opposite effects of Apoer2$^{\Delta 16+19}$ (up, OPRK1, RCC2; down, ROCK1, SLC1A1, ARID1B, BRWD1, DSP, KDM4B, ND6, RALGAPA2, ZNF644), 4 were common between Apoer2$^{\Delta 16+19}$ and Apoer2$^{\Delta 16\Delta 19}$ with opposite effect in Apoer2^{cKO} (ACTA2, SETD2, NCOA2), and 2

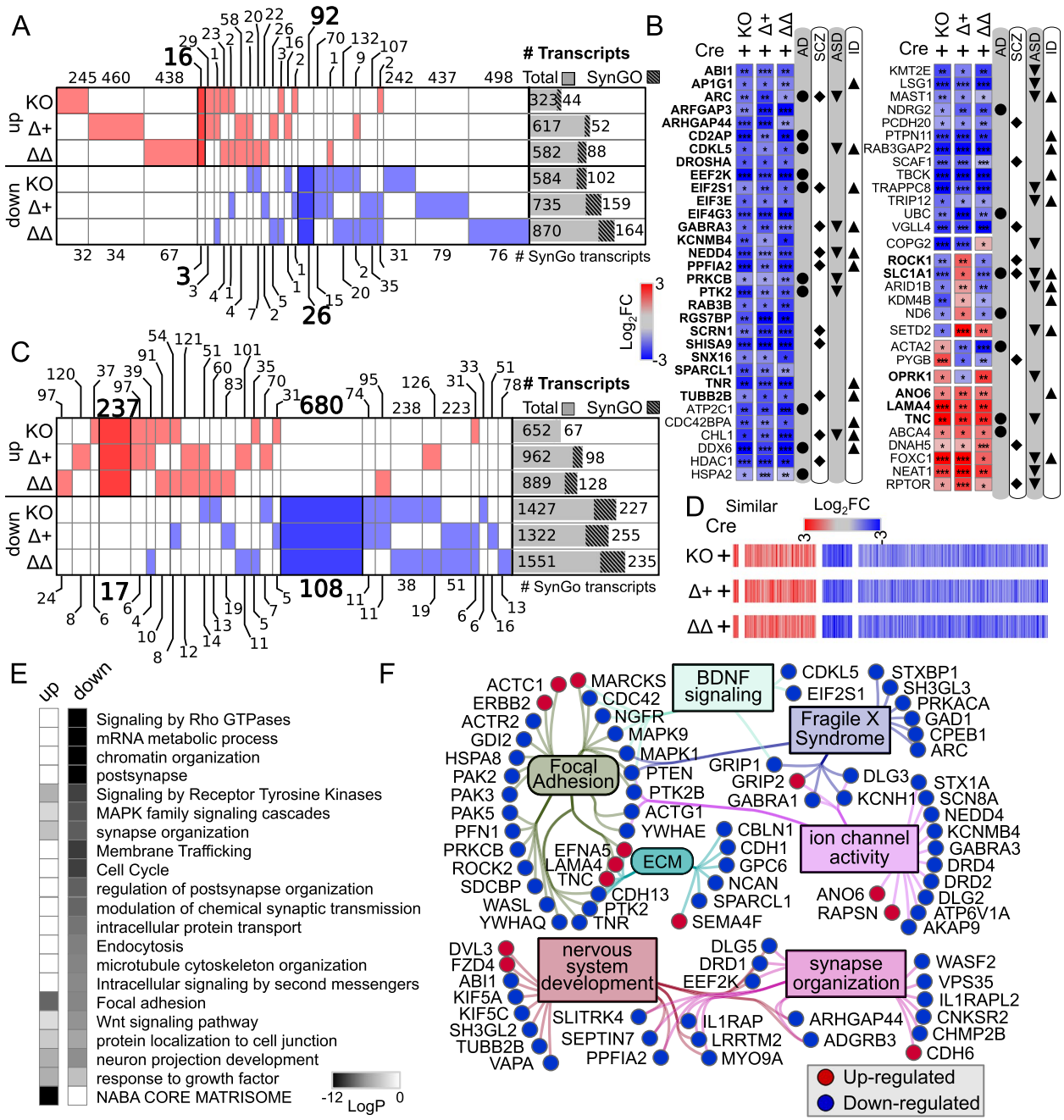

Fig. 2 Basal translatome differences in Apoer2^{cKO} and cleavage-deficient hippocampi. **A**, **B** Supervenn and heatmap depicting the overlap of transcripts significantly altered in Apoer2 transgenic mice compared to Apoer2^{WT}. **A** Translatome overlap of transcripts significantly (*p*-value< 0.05, $|\log_2 FC| > 0.58$) altered in the Apoer2 KI/cKO genotypes compared to Apoer2^{WT}. **B** Heatmap of the 53 translating SynGO (bolded) and disease-related transcripts (symbols) significantly altered in all three Apoer2 KI/cKO compared to Apoer2^{WT}. **C** Expanded translatome overlap of the ~3,000 transcripts altered in the Apoer2 KI/cKO genotypes compared to Apoer2^{WT} ($|\log_2 FC| > 0.58$, *p*-value<0.05 in at least one). **D** Heatmap demonstrating the $\log_2 FC$ of expanded basal translatome in Apoer2^{cKO} and cleavage-deficient hippocampi. **E** Enrichment analysis of the transcripts in Panel D. **F** Diagram depicting the SynGO transcripts differentially-translated in the Apoer2 KI/cKO (Panel D) compared to Apoer2^{WT} (up, red circles; down, blue circles) in the network from Fig. 1F. AD, Alzheimer's disease; SCZ, schizophrenia; ASD, autism spectrum disorders; ID, intellectual disability

were common between Apoer2^{cKO} and Apoer2$^{\Delta16+19}$ with opposite effect in Apoer2 $^{\Delta16\Delta19}$ (up, RASAL2; down, COPG2) (Fig. 2B). This demonstrates the ability of exon 19 and splicing to affect synaptic homeostasis in the absence of its normal γ-secretase mediated cleavage.

As all Apoer2 KI/cKO mice lack the release of the Apoer2-ICD, we expected to find more than just 4.2% of the differentially regulated transcripts in common between them when compared to Apoer2^{WT}. To find similar regulatory modules within these >2000 transcripts only, we reduced our criteria within these genes to $|\log_2 FC| > 0.5$ (Fig. 2C, D). With this reduced criterion, we identified 237 up- and 680 down-regulated transcripts in all three Apoer2 KI/cKO (605 total, Figure S4A, B, Table S5). Eighty-one of these are annotated in GSEA [62, 77] as transcription factors (Figure S3). Further, several of these genes are also associated with LTP (Figure S4C). Overall, these similarly regulated transcripts can be grouped into 20 functional enrichments across the three Apoer2 KI/cKO lines (Fig. 2E, Table S5). Focal adhesion transcripts were both up- and down-regulated. The other top enrichments for up-regulated transcripts were response to growth factor, neuron projection development, and matrisome. The top enrichments for down-regulation were post-synaptic transcripts, Signaling by Rho GTPases, and mRNA metabolic process (Fig. 2E, Table S5).

There were 17 up- and 108 down-regulated synaptic translating transcripts with similar differential regulation in the Apoer2 KI/cKO lines compared to wild-type controls, suggesting potential key transcripts that are regulated by the Apoer2-ICD. Eighty-five of these transcripts were in our minimal synaptic network from Fig. 1F with 13 transcripts up- and 72 down-regulated (Fig. 2F). Of the other SynGO annotated transcripts not in the network were 4 up- and 36 down-regulated.

Only 416 transcripts were not shared between at least two of the genotypes. Of the 416 differentially changed in only one genotype, Apoer2^{cKO} has 37 up- and 33 down-regulated (up-regulation in neuron death: APOE, CASP3, MAPK8, TFAP2B), Apoer2 $^{\Delta16+19}$ has 120 up- and 51 down- regulated, and Apoer2 $^{\Delta16\Delta19}$ has 97 up- and 78 down-regulated. The differential regulation of these synaptic translating transcripts could provide insight into the differential phenotypes observed in these mouse lines.

Apoer2-ICD regulation in the Apoer2^{WT}

Across all Apoer2^{WT} conditions overexpressing either Apoer2-ICD, there were 1,034 differentially regulated transcripts (Fig. 3, S3B, Table S1). Compared to the Apoer2^{WT} injected with lentivirus expressing only Cre, the inclusion of one of the Apoer2-ICDs up- and down-regulated 718 and 314 transcripts, respectively. Only 2 transcripts were regulated in opposite directions by the two ICDs with both up-regulated by Apoer2-ICD[+19] and down with Apoer2-ICD[Δ19] (DYNLRB2, KBTBD12). Of the up-regulated transcripts, 612 are augmented by both Apoer2-ICDs, 49 by Apoer2-ICD[+19], and 57 by Apoer2-ICD[Δ19]. One of the transcripts up-regulated by only the Apoer2-ICD[+19] is LRP3, whose expression is increased by Apoer2 and is reduced in the frontal cortex of postmortem AD brains [19]. The top functional enrichment categories for these up-regulated transcripts were post-synapse, cell junction organization, and cellular component morphogenesis (Figure S5A, Table S6).

Of the 314 down-regulated transcripts, 203 are reduced by both Apoer2-ICDs, 6 by Apoer2-ICD[+19], and 105 by Apoer2-ICD[Δ19]. The top functional enrichment categories for these down-regulated transcripts were cell surface receptor signaling pathways involved in cell-cell signaling, nervous system development, and cellular component morphogenesis (Figure S5A, Table S6). Seven of these genes are Alzheimer's disease-related, six are down-regulated with both Apoer2-ICDs (COX7A2L, FZD2, KIF5A, MAP2K2, PSENEN, RAF1) and one with only the Apoer2-ICD[Δ19] (SLC39A9). Twelve of the down-regulated transcripts are schizophrenia-related with regulation of 10 by both Apoer2-ICDs (ARHGAP18, GSTM1, HAGH, HDAC1, HTR1F, JAG1, NDEL1, NGFR, S100B, TRPM1) and 2 with only the Apoer2-ICD[Δ19] (RASD2, SMAD5).

Approximately 12% of these transcripts altered in the Apoer2^{WT} hippocampus with one or both of the Apoer2-ICD splice variants are annotated in the SynGO database. Most of these are up-regulated with 86 up-regulated by both, 6 by only the Apoer2-ICD[+19], and 4 by only the Apoer2-ICD[Δ19]. Of those down-regulated, 19 are down-regulated by both Apoer2-ICDs, only one by Apoer2-ICD[+19], and 3 by Apoer2-ICD[Δ19]. Eighty-nine of these SynGO annotated transcripts made it into our minimal synaptic network from Fig. 1F with 70 transcripts up- and 12 down-regulated by both Apoer2-ICDs (Fig. 3C, D). Only 14 transcripts are uniquely regulated by just one of the ICDs (Fig. 3C, D). Thirty of the ICD-regulated synaptic transcripts did not fall into our gene enrichment network (Fig. 3D). Twenty were up-regulated with 16 by both and 2 each by either ICD only. The other 10 SynGO transcripts not represented in the minimum network were down-regulated with 7 by both, 1 by Apoer2-ICD[+19], and 2 by Apoer2-ICD[Δ19]. These down-regulated transcripts consisted of 6 integral synaptic vesicle components (SYT12, SV2B, STX6, PTPRN2, VAMP3, SVOP$^{[\Delta19]}$).

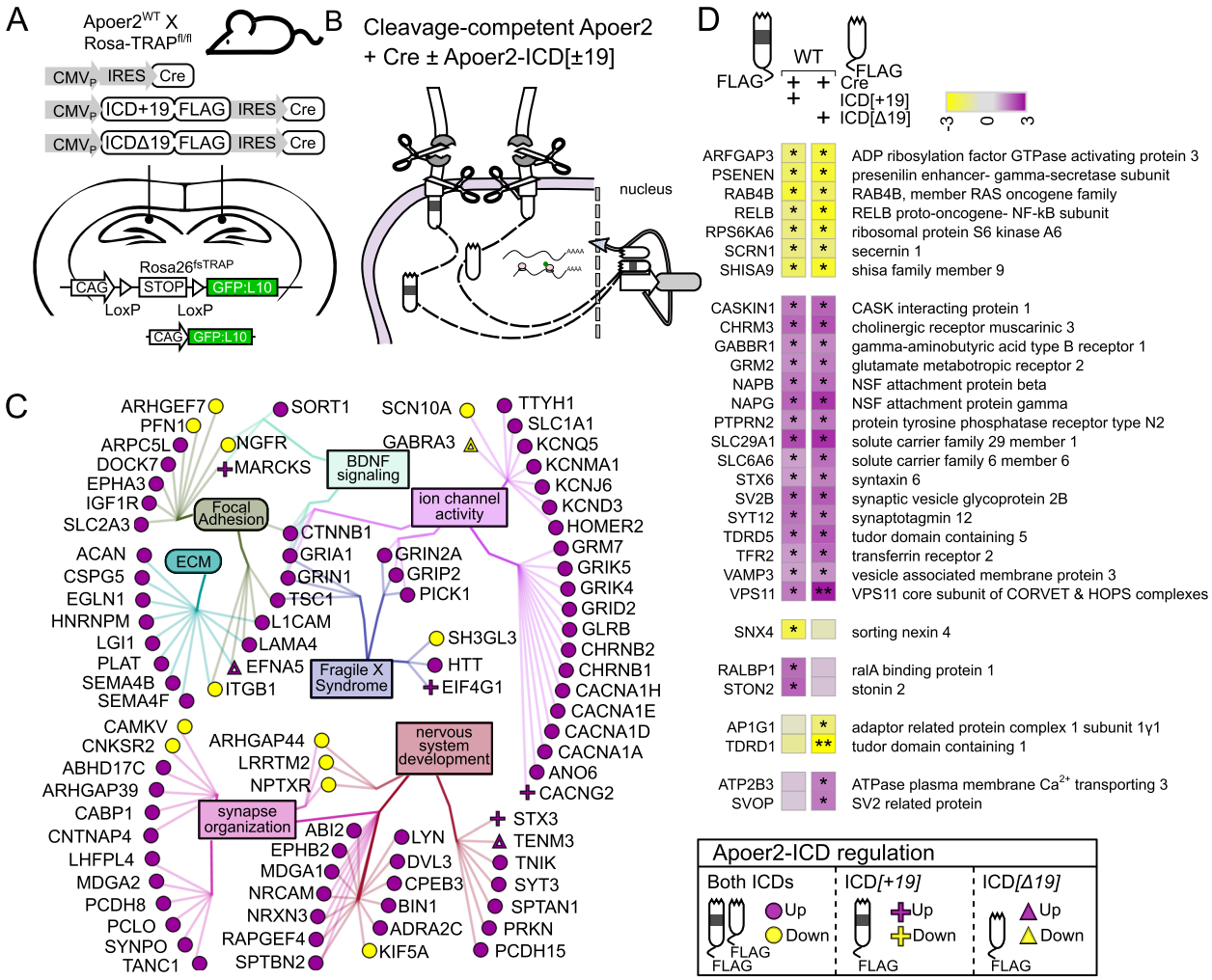

Fig. 3 Synaptic effects of overexpressing either Apoer2-ICD in Apoer2^{WT}. **A**, **B** Schematic representation of the experiment. **C** Diagram depicting the up- (purple symbols) and down- (yellow symbols) regulated transcripts by both ICDs in the same direction (circles), ICD[+19] (plus-sign) or ICD[Δ19] (triangles). **D** Heatmap of the $\log_2$FC differentially-transcribing transcripts in Apoer2^{WT} with either Apoer2-ICD from the network in Fig. 1F. Heatmap displaying the $\log_2$FC expression of the synaptic transcripts not represented in the networks in Panels **A** and **B**, respectively. *p<0.05, **p<0.01

Apoer2-ICD regulation in the Apoer2^{cKO}

Across all Apoer2 conditional knockout conditions there are 1,475 translating transcripts differentially regulated, with 60% regulated by the lack of Apoer2 and 40% a result of expression of exogenous Apoer2-ICD. Compared to Apoer2^{WT} injected with lentivirus expressing Cre-only, the Apoer2^{cKO} injected with Cre has 323 up- and 584 down-regulated genes (907 total) and 146 of them are annotated in SynGO (44 up; 102 down). Of the ribosome loaded transcripts differentially regulated between Apoer2^{WT} and Apoer2^{cKO} hippocampi, ~94% are rescued, leaving only 32 transcripts not rescued by one of the Apoer2-ICDs. Of those rescued, 233 of the 323 up-regulated transcripts were rescued by both Apoer2-ICDs (38 synaptic), while 21 and 31 were rescued by only the Apoer2-ICD[+19] or [Δ19], respectively (Table S2). The top functional enrichment categories for these up-regulated transcripts were extracellular matrix/focal adhesion and response to growth factor (Figure S5B, Table S7).

Of the down-regulated transcripts, 120 are not rescued by either of the Apoer2-ICDs (top 10: SLITRK4, ENPP2, KDM3A, DRD1, COPG2, RAB3GAP2, CD2AP, PPFIA2, UBR5, ADGRB3). Of the ~80% rescued, 271 of the 584 down-regulated transcripts were rescued by both Apoer2-ICDs, while 14 and 175 were rescued by only the Apoer2-ICD[+19] or [Δ19], respectively (Table S2). The top functional enrichment categories for these

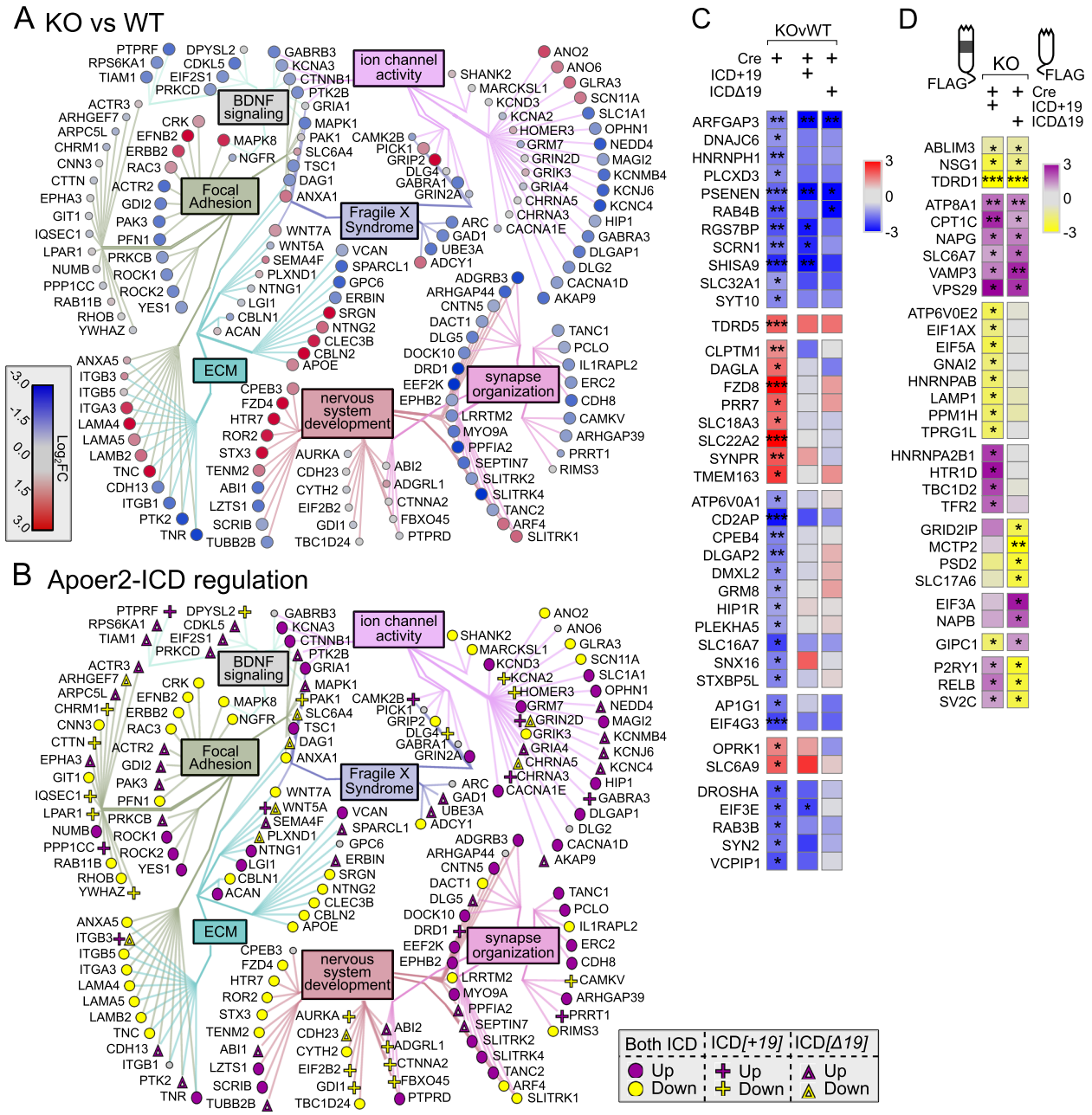

Fig. 4 Synaptic effects of Apoer2-ICD in Apoer2^{cKO}. **A**, **B** Diagrams depicting the transcripts differentially-translated in the Apoer2^{cKO} at baseline (Cre-only) compared to Apoer2^{WT} (up, red circles; down, blue circles) (**A**) or differentially-translated in Apoer2^{cKO} neurons expressing either ICD[+19] (plus-sign) or ICD[Δ19] (triangles) compared to the baseline Apoer2^{cKO} in the network from Fig. 1F (up, purple symbols; down, yellow symbols) (**B**). Note in Panel B, transcripts regulated by both ICDs in the same direction are depicted with circles and those differentially regulated by either the ICD[+19] or ICD[Δ19] are represented by plus-signs or triangles, respectively. **C**, **D** Heatmap displaying the $\log_2$FC expression of the synaptic transcripts not represented in the networks in Panels **A** and **B**, respectively. *p<0.05, **p<0.01

down-regulated transcripts were positive regulation of organelle organization, supramolecular fiber (actin) organization, and small GTPase mediated signal transduction (Figure S5B, Table S7). This demonstrates the sufficiency of the Apoer2-ICD to regulate synaptic ribosome loaded mRNA abundance in the absence of the full-length receptor.

Within our minimal synaptic network from Fig. 1F, there are 164 transcripts regulated overall in the Apoer2^{cKO} conditions (Fig. 4A, B) with 106 transcripts

either up- or down-regulated (33 and 73, respectively) compared to the Apoer2^{WT}. The other 58 transcripts are regulated by one or both Apoer2-ICDs independent of the basal effect of Apoer2-ICD deficiency (genotype-independent). Of those 106 basal translating transcripts differentially regulated in the Apoer2^{cKO} compared to the Apoer2^{WT}, only 16 down-regulated transcripts are not rescued by either Apoer2-ICD (Fig. 4A, B, Table S2). Of those rescued, all of the up-regulated transcripts were rescued by both Apoer2-ICDs, while half of the down-regulated transcripts were rescued by both Apoer2-ICDs and 3 or 27 by only the Apoer2-ICD[+19] or Apoer2-ICD[Δ19], respectively. Gene enrichment revealed up-regulation in focal adhesion and both up- and down-regulation in synapse/nervous system development with increased ribosome association of transcripts coding Wnt-binding proteins (FZD4, FZD8, ROR2) and decreases in transcripts involved in dendrite morphology (ARHGAP44, LZTS1, NEDD4, OPHN1, ROCK2, SEPTIN7, TANC1, UBE3A) (Figure S5B, Table S7).

Of the 54 synaptic translating transcripts within the minimal network differentially regulated independent of the basal genotype, both Apoer2-ICDs similarly affected the ribosome association of 24 transcripts with 10 up and 14 down-regulated, while ribosome association of 4 and 6 up-regulated or 16 and 5 down-regulated transcripts were regulated by only the Apoer2-ICD[+19] or Apoer2-ICD[Δ19], respectively. Three transcripts are differentially translated in opposite directions by the two Apoer2-ICDs and each are up with Apoer2-ICD[+19] and down with the Apoer2-ICD[Δ19] (GRIN2D, ITGB3, P2RY1) (Fig. 4B).

Synaptic effect of cleavage-resistant Apoer2

In neurons lacking Apoer2, synapse number decreases, and those lacking cleavage of Apoer2 have increased synapse number with reduced synaptic function. These cleavage-resistant variants can also impart additional effects depending on the presence or absence of the proline-rich domain. When this ICD domain is absent, all the above-mentioned effects are further exacerbated, while its presence imparts a Reelin-independent increase in long-term potentiation [86]. To probe the effects of the ICD variants on synaptic ribosome-associated transcripts *in vivo*, we compared the baseline effects of cleavage-resistant Apoer2 on translating transcripts, as well as the effect of Apoer2-ICD reintroduction. As expected, we observed up-regulation of Apoer2 in both Apoer2 KI mice lacking the OLS (~4-fold increase) and down-regulation in the conditional Apoer2^{cKO} (Additional file 2: Tables S2-4).

Apoer2-ICD regulation in the Apoer2$^{\Delta 16+19}$

Across all Apoer2$^{\Delta 16+19}$ conditions, there are 1,944 translating transcripts differentially regulated, with 70% regulated by genotype and 40% a result of expression of exogenous Apoer2-ICD (Fig. 1C, D, Figure S2D-F). Compared to Apoer2^{WT}, the Apoer2$^{\Delta 16+19}$ injected with Cre alone has 617 up- and 735 down-regulated genes (1352 total, Table S3), and the ribosomal-association of the majority of these were normalized by one or both Apoer2-ICDs (85 and 75%, respectively). Of the up-regulated transcripts, 95 are not rescued by either of the Apoer2-ICDs (including Apoer2, shown as LRP8 in Fig. 5) with 9 annotated in SynGO. Of the 522 up-regulated transcripts rescued, 361 were rescued by both Apoer2-ICDs, while 96 and 51 were rescued by only the Apoer2-ICD[+19] (synaptic transcripts : ROCK1, NAPB) or [Δ19] (synaptic transcripts: ACTC1, ADRA1A, CDH6, EFNA5, GRIN2D, PLCG1, PRKCD, PUM2), respectively (Table S3). The top functional enrichment categories for these up-regulated transcripts were cell junction organization, head development, and signaling by receptor tyrosine kinases (Figure S5C, Table S8).

Of the down-regulated transcripts, 551 (~75%) are rescued by either Apoer2-ICD. 152 of the 735 down-regulated transcripts were rescued by both Apoer2-ICDs, while 52 and 347 were rescued by only the Apoer2-ICD[+19] or [Δ19], respectively (Table S3). The top functional enrichment categories for these down-regulated transcripts were synaptic signaling, cell cycle, and post-synapse (Figure S5C, Table S8).

Within our minimal synaptic network from Fig. 1F, there are 211 transcripts regulated overall in the Apoer2$^{\Delta 16+19}$ conditions (Fig. 5A-D). 146 transcripts are either up- or down-regulated (103 and 43, respectively), and all except 7 of the up- and 25 of the down-regulated transcripts are rescued by reintroduction of the Apoer2-ICD. Within this group, we observed increased ribosomal-association of transcripts modulating synaptic transmission (AKAP12, DNM1, GRIN2D, GSK3B, HOMER1, HTR1A, LGI1, NF1, PICK1, PLCG1, RAB8A, RAPSN) and decreased ribosomal-association transcripts coding for regulators of translation (CPEB1, EEF2K, EIF2B2, EIF2S1, EIF4E) as well as memory impairment (BDNF, DPYSL2, DRD1, DRD2, FYN, NGFR, NOS1, PTEN, SYN1, VPS35). Of the 114 rescued, 41 were rescued by both Apoer2-ICDs, 18 by only the Apoer2-ICD[+19], and 55 by only the Apoer2-ICD[Δ19]. The up-regulated transcripts fall mostly under the Fragile X Syndrome category. We observed a general down-regulation in focal adhesion transcripts, 7 of which are involved in integrin signaling (ITGB5, ACTG1, ACTN1, CDC42, FYN, MAPK3, RAC1, RAP1B), as well as synapse/neuron organization including cytoskeleton-binding proteins (ACTN1, ARC, DLG5, DPYSL2, FYN, HNRNPK, KIF5A, SDCBP, SYN1, VAPA).

Of the 65 other ribosomal-associated transcripts within the minimal synaptic network affected by the

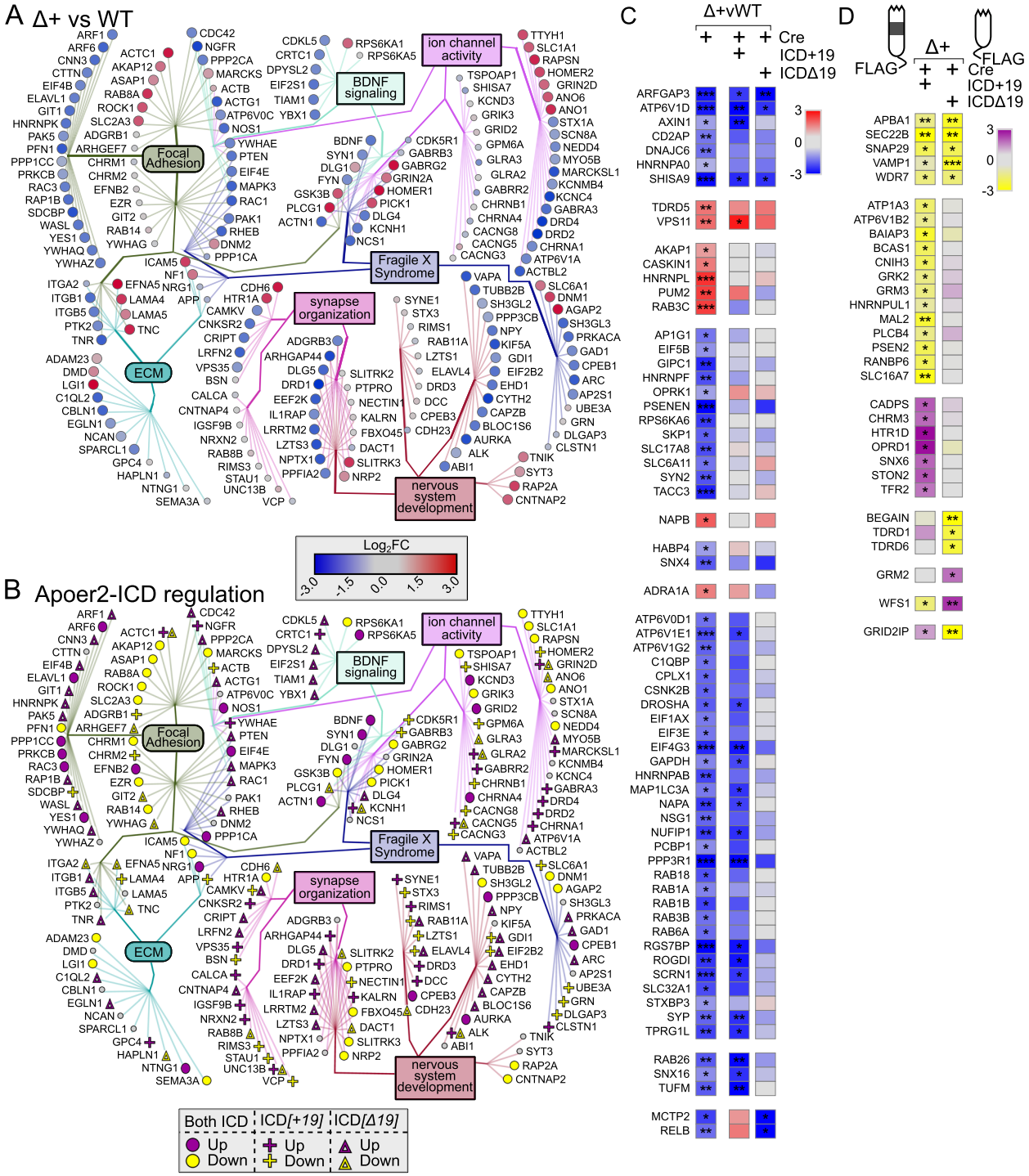

Fig. 5 Synaptic effects of Apoer2-ICD in Apoer2$^{\Delta 16+19}$. **A**, **B** Diagrams depicting the transcripts differentially-translated in the Apoer2$^{\Delta 16+19}$ knockin at baseline (Cre-only) compared to Apoer2^{WT} (up, red circles; down, blue circles) (**A**) or differentially-translated in Apoer2$^{\Delta 16+19}$ neurons expressing either ICD[+19] (plus-sign) or ICD[Δ19] (triangles) compared to the baseline Apoer2$^{\Delta 16+19}$ in the network from Fig. 1F (up, purple symbols; down, yellow symbols) (**B**). Note in Panel **B**, transcripts regulated by both ICDs in the same direction are depicted with circles and those differentially regulated by either the ICD[+19] or ICD[Δ19] are represented by plus-signs or triangles, respectively. **C**, **D** Heatmap displaying the $\log_2$FC expression of the synaptic transcripts not represented in the networks in Panels **A** and **B**, respectively. *p<0.05, **p<0.01, ***p<0.001

Apoer2-ICDs independent of their baseline differences to Apoer2^{WT}, both ICDs up-regulate 9 and down-regulate 8 transcripts. The Apoer2-ICD[+19] and Apoer2-ICD[Δ19] independently regulate 35 and 16 transcripts, respectively. Five transcripts are differentially translated in opposite directions by the two Apoer2-ICDs, 3 are up with Apoer2-ICD[+19] and down with the Apoer2-ICD[Δ19] (CACNG5, GLRA2, UNC13B), while ELAVL4 and RAB11A are down with Apoer2-ICD[+19] and up with the Apoer2-ICD[Δ19] (Table S3).

Apoer2-ICD regulation in the Apoer2$^{\Delta16\Delta19}$

Across all Apoer2 $^{\Delta16\Delta19}$ conditions, there are 2317 translating transcripts differentially regulated. Compared to Apoer2^{WT}, the Apoer2$^{\Delta16\Delta19}$ mice injected with Cre have 582 up- and 872 down-regulated genes (1454 total, Figure S2G-I, Table S4). Of the up-regulated transcripts, only 55 are not rescued by one of the Apoer2-ICDs. Of the 91% rescued, 373 of the 582 up-regulated transcripts were rescued by both Apoer2-ICDs, while 34 and 120 were rescued by only the Apoer2-ICD[+19] or [Δ19], respectively (Table S4). The top functional enrichment categories for these up-regulated transcripts were post-synapse, cellular component morphogenesis, and axon (Figure S5D, Table S9).

Of the down-regulated transcripts, 667 are rescued by one of the Apoer2-ICDs. Of the 76.5% rescued, 294 of the 872 down-regulated transcripts were rescued by both Apoer2-ICDs, while 36 and 377 were rescued by only the Apoer2-ICD[+19] or [Δ19], respectively (Table S4). The top functional enrichment categories for these transcripts were post-synapse, Rho GTPases signaling, and cellular component morphogenesis (Figure S5D, Table S9).

Within our minimal synaptic network from Fig. 1F, there are 241 SynGO transcripts regulated overall in the Apoer2$^{\Delta16\Delta19}$ conditions (Fig. 6). One hundred and sixty-three transcripts are either up- or down-regulated (101 and 62, respectively), and all except 2 and 24 of the up- and down-regulated transcripts, respectively, are rescued by reintroduction of the Apoer2-ICD. Of the 172 rescued, 82 were rescued by both Apoer2-ICDs, 2 by only the Apoer2-ICD[+19], and 53 by only the Apoer2-ICD[Δ19].

Of the 78 other transcripts within the minimal synaptic network which are affected by the Apoer2-ICDs independent of their baseline differences to Apoer2^{WT}, both ICDs up-regulate 11 and down-regulate 2 transcripts. The Apoer2-ICD[+19] and Apoer2-ICD[Δ19] independently regulate 24 and 34 transcripts, respectively. Five transcripts are differentially regulated in opposite directions by the two Apoer2-ICDs, 5 are up with Apoer2-ICD[+19] and 5 are down with the Apoer2-ICD[Δ19] (ABL1, ERBB2, LPAR1, SCN10A, WNT5A), while ACTR3 and DLG1 are down with Apoer2-ICD[+19] and up with the Apoer2-ICD[Δ19] (Fig. 6A, B, Table S4).

Apoer2-ICD regulation of key AD risk genes and members of the Reelin signaling pathway

The inclusion of exon 19 in the Apoer2-ICD is protective against AD pathogenesis, so we next assessed the effect of the Apoer2-ICD splice variants on the regulation of translating transcripts of key AD risk genes [39]. To date, there are ~90 known AD genetic risk loci with more than 100 potential risk genes [3, 46, 87]. Of these, 34 transcripts are differentially translated in one or more experimental conditions compared to Apoer2^{WT} (Fig. 7A). Over 50% of these play a critical role in APP/Aβ metabolism, including APP itself, as well as three gamma-secretase subunits (PSEN1, PSEN2 and APH1B). Ten of these are involved in Aβ toxicity or clearance (ABCA7, ACE, BIN1, CD2AP, CR1, CTSB, CTSH, GRN, PTK2B and SORL1), and nine play a role in tau toxicity. Other functional roles of these AD risk genes include regulation of immune response, endocytosis, cytoskeleton, neuron projection, and synaptic function. In Apoer2^{cKO} and cleavage-deficient lines, only CD2AP is significantly regulated in the same direction (down). If we consider transcripts that are significantly altered in at least one Apoer2^{cKO} or cleavage-deficient line, we find four with similar down-regulation (log2FC <= -0.5): CR1, FERMT2, PLCG2 and PTK2B. There are no up-regulated AD risk transcripts significantly or similarly up-regulated in all three deficient lines.

A recent genetic linkage analysis implicates the Reelin signaling pathway in AD pathogenesis [7]. When we assess the effect of the Apoer2-ICD across all conditions on the ribosome-associated transcripts of these members of the Reelin signaling pathway, nearly half of the core Reelin signaling pathway transcripts are altered (Fig. 7B).RELN itself was upregulated in all Apoer2 KI/cKO models (Table S10), but only significantly so in Apoer2 $^{\Delta16\Delta19}$ hippocampi. This is not surprising considering all Apoer2 KI/cKO mice lack the Apoer2-ICD, which we and others have shown to down-regulate RELN expression (Figure S1) [1]. When we look for commonalties between the two Apoer2 KI lines, we observe similar changes in the core receptor signaling pathway (Fig. 7B) with the expected up-regulation of LRP8 along with up-regulation of GSK3B and CBL and down-regulation of FYN. As for dissimilarities between the two Apoer2 KI lines, we observe opposite regulation of CDK5, ITGB1, and YES1 translating transcripts with each down- and up-regulated in Apoer2$^{\Delta16+19}$ and Apoer2$^{\Delta16\Delta19}$, respectively. Between the Apoer2^{cKO} and Apoer2$^{\Delta16+19}$, each have similar down-regulated translating transcripts of ITGB1, RAPGEF1, and YES1 and up-regulation of

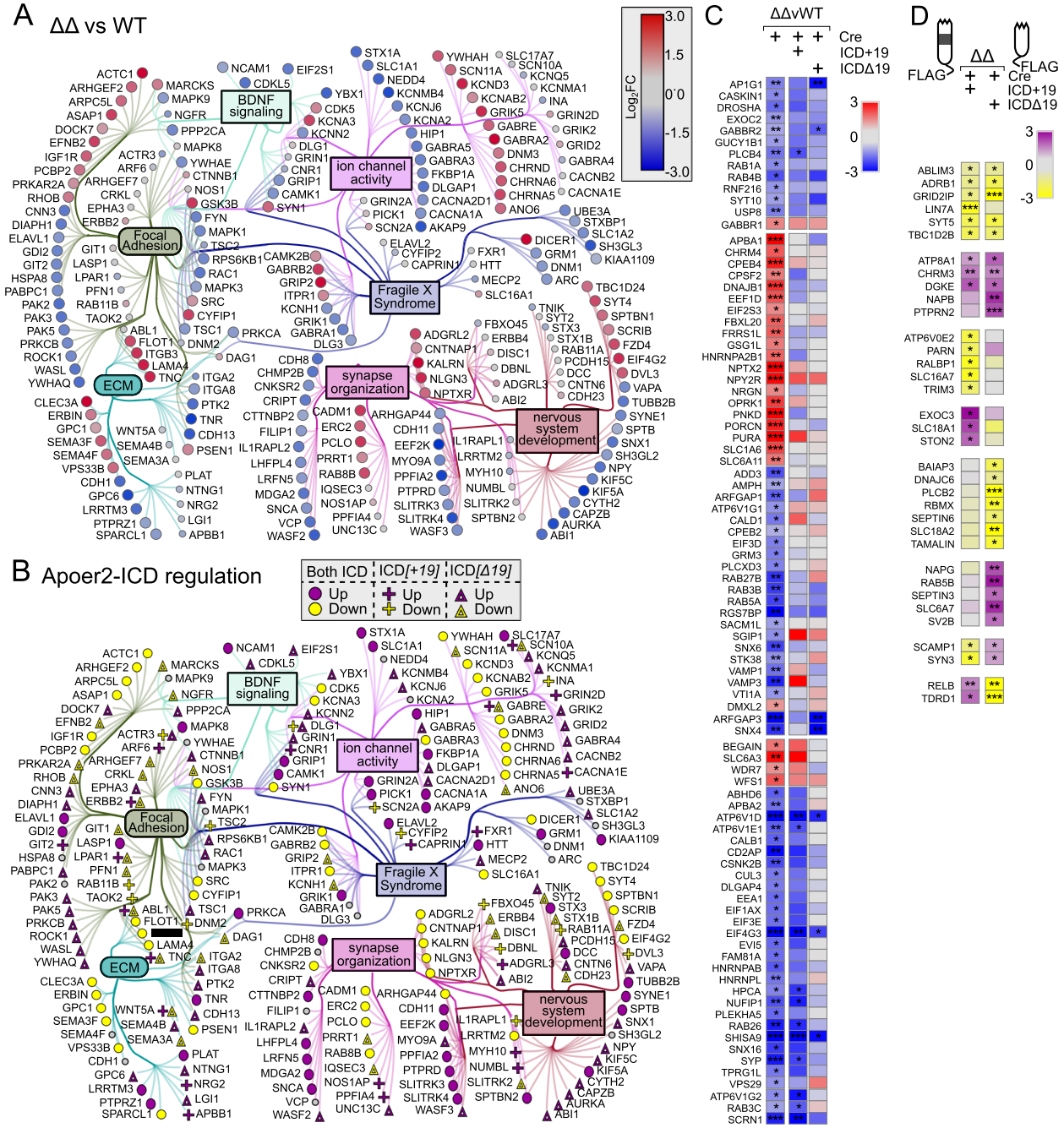

Fig. 6 Synaptic effects of Apoer2-ICD in Apoer2$^{\Delta16\Delta19}$. **A**, **B** Diagrams depicting the transcripts differentially-translated in the Apoer2$^{\Delta16\Delta19}$ knockin at baseline (Cre-only) compared to Apoer2^{WT} (up, red circles; down, blue circles) (**A**) or differentially-translated in Apoer2$^{\Delta16\Delta19}$ neurons expressing either ICD[+19] (plus-sign) or ICD[Δ19] (triangles) compared to the baseline Apoer2$^{\Delta16\Delta19}$ in the network from Fig. 1F (up, purple symbols; down, yellow symbols) (**B**). Note in Panel **B**, transcripts regulated by both ICDs in the same direction are depicted with circles and those differentially regulated by either the ICD[+19] or ICD[Δ19] are represented by plus-signs or triangles, respectively. **C**, **D** Heatmap displaying the $\log_2$FC expression of the synaptic transcripts not represented in the networks in Panels **A** and **B**, respectively. *p<0.05, **p<0.01, ***p<0.001

ITGA3. Alternatively, ribosome association of GRIN2A and PIK3R1 transcripts is up-regulated in Apoer2$^{\Delta16+19}$ and down-regulated in Apoer2^{cKO}. The only shared similarity unique to the Apoer2$^{\Delta16\Delta19}$ and Apoer2^{cKO} cells is up-regulation of CRK translating transcripts. None of the transcripts are regulated in only the Apoer2$^{\Delta16+19}$, while MAPK8 is up-regulated in Apoer2^{cKO} and ARHGEF2 and SRC are up-regulated in Apoer2 $^{\Delta16\Delta19}$ alone. Overall, this

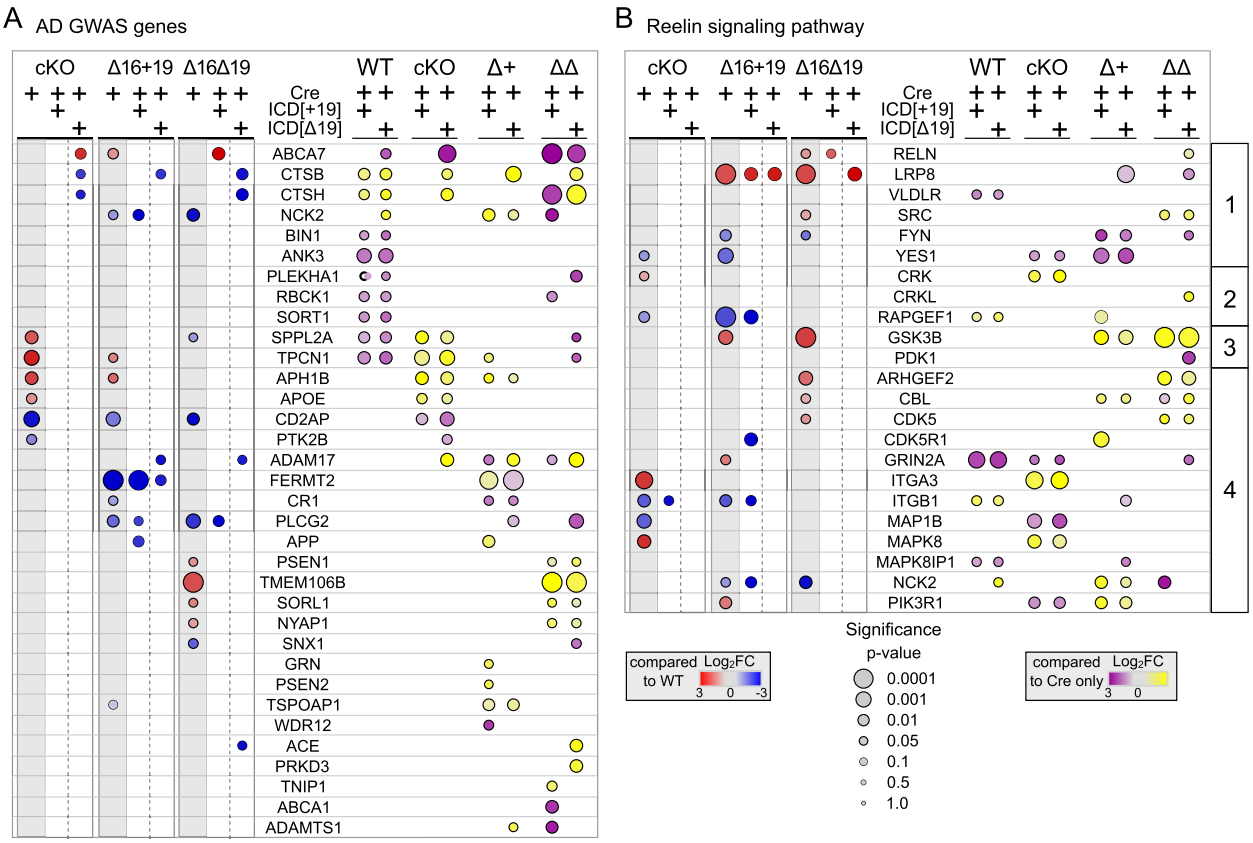

Fig. 7 Apoer2-ICD regulation of AD GWAS and Reelin signaling transcripts. Heatmaps depicting the log_2FC of translating AD GWAS (**A**) or Reelin signaling pathway (**B**) transcripts between the Apoer2cKO/KI neurons expressing only Cre or Cre with either Apoer2-ICD compared to Apoer2^{WT} expressing only Cre (left panels of A,B) or between neurons expressing either ICD[+19] or ICD[Δ19] compared to the Cre-only translation within each genotype (right panels of A,B). **B** Reelin pathway transcripts are sorted into four groups: the core Reelin receptor complex and associated tyrosine kinases (1), the signaling pathway regulating cadherin trafficking (2), the signaling pathway regulating tau (MAP1B) phosphorylation (3), and the other members of the canonical Reelin pathway (4). Significance is represented by the size of the node

analysis demonstrates several AD risk genes are regulated either by Apoer2 and/or by the Apoer2-ICD, implicating Apoer2 and its alternative splicing in AD pathogenesis and suggesting the Apoer2/Reelin pathway is a rational target for possible AD therapies.

Discussion

Apoer2 signaling is critical for brain development, synapse maturation and maintenance as well as function, and inclusion of exon 19 is protective against AD-related synaptic changes [2, 26, 30, 65, 69, 75, 86]. Recently, a Reelin gain-of-function mutation has been reported to be protective against early-onset AD [56], thus directly implicating the Reelin/Apoer2 pathway in AD pathogenesis. We know that the abundance of Apoer2 can proportionately regulate synapse number [26, 86], and its cleavage can block extracellular signaling as well as transcription by the release of the ICD [1, 48, 81].

As transcription does not always reflect translating transcripts, we sought to uncover how the Apoer2-ICD regulates the synaptic translatome using a multi-model approach with three genetic Apoer2 mouse lines – each lacking the Apoer2-ICD. Here we demonstrate a large network of differentially regulated translating transcripts where the Apoer2-ICD is either not present or not released. This network comprises 15% of all the annotated mouse genes. Of these, half were significantly altered by just the loss of the Apoer2-ICD release and the majority were rescued by reintroducing either Apoer2-ICD with or without the alternatively spliced exon 19. Without the Apoer2-ICD, approximately 30% of the differentially regulated translating transcripts were similarly altered across all Apoer2^{cKO} and cleavage-deficient mouse lines – mice with very different phenotypes – suggesting a common Apoer2-ICD regulatory module. From cell adhesion to synaptic scaffolds and the core machinery of chemical neurotransmission, the Apoer2 translatome spans almost all aspects of the synapse and intersects with many brain disorders (AD, schizophrenia, bipolar disorder, autism, epilepsy, and

depression) unveiling an expansive synaptic role for Apoer2.

Part of this module is enriched in integrins, collagens, laminins, and a variety of cadherin- and cytoskeleton-binding proteins (Fig. 2), which are key players in focal adhesion. Focal adhesions link the extracellular matrix (ECM) to the inside of the cell through complex intracellular interactions. Part of the ECM is suggested to mark the location of eliminated synapses [42]. Considering that neurons of young Apoer2 knockout mice have fewer synapses along with our observation of enhanced ribosome association of ECM transcripts in the Apoer2^{cKO} and the lack of ECM-specific enrichment in any other condition, it is possible these transcripts could truly act as placeholders for the synapses lost upon deletion of Apoer2 [26].

Reelin is known to interact with not only NMDA receptors but also integrins and other critical downstream signaling pathways including those regulating the cytoskeleton [22]. When Reelin's protein abundance is reduced in neurons, overall translating transcript numbers are also reduced. This includes the regulation of the critical regulator of synaptic homeostasis, translation, and cytoskeletal dynamics - activity-regulated cytoskeletal protein (ARC). Reelin signaling leads to the release of the Apoer2-ICD, and in this study, we observed down-regulation of ARC in the translatomes of all Apoer2-ICD cKO/KI genotypes, further implicating the Reelin/Apoer2 pathway in ARC signaling. Likewise, Reelin, in conjunction with integrins, enhances ARC translation in an mTOR-dependent manner [25]. We observed decreased ribosome associated transcripts of several translation regulators across all genotypes,however, whether these effects are a product of overall reduced Reelin function or a key component of how the lack of the Apoer2-ICD impacts protein translation/mRNA transcription could not be deduced.

Translatome differences between Apoer2^{cKO} and cleavage-deficient mouse lines: Clues to phenotypic differences

Understanding the subtle differences between the Apoer2^{cKO} and cleavage-deficient mouse models could be the key to unlocking unknown functions of Apoer2 at the synapse. The hippocampal neurons in the uncleavable Apoer2 lines have reduced synaptic transmission despite increased synapse number. The additional loss of exon 19 further increases synaptic density and suppresses synaptic function, all of which are rescued by reducing Apoer2 protein abundance [86]. Between the uncleavable Apoer2 lines (Apoer2$^{\Delta 16\pm 19}$), 15 synaptic transcripts have similar changes in translating transcripts compared to Apoer2^{WT} (up: ACTC1, ANO6, ASAP1, GSK3B, LAMA4, LRP8, MARCKS, TNC,down: ATP6V1D, ATP6V1E1, AURKA, EEF2K, EIF4G3, ELAVL1, KIF5A, RGS7BP, SCRN1, SHISA9, SYP) and 5 were significantly regulated in opposite directions (SYT1, SLC6A11 and HNRNPL, ROCK1, SLITRK3). Of these, six regulate translation or mRNA splicing.

Ribosome-associated transcripts of ROCK1 and SLITRK3 are up-regulated in the Apoer2$^{\Delta 16+19}$ mouse line and down in the Apoer2 $^{\Delta 16\Delta 19}$ mouse line, while SYT1 and SLC6A11 are down-regulated in the Apoer2$^{\Delta 16+19}$ mouse line and up in the Apoer2 $^{\Delta 16\Delta 19}$ mouse line. SLITRK3 promotes inhibitory synapse formation and SLC6A11 is a GABA transporter, suggesting GABAergic synaptic input may be elevated in the hippocampi of Apoer2$^{\Delta 16+19}$ mice and reduced in Apoer2 $^{\Delta 16\Delta 19}$ mice [53, 80, 89]. This suggests a potential difference in GABAergic input between the uncleavable Apoer2 KI hippocampal neurons, possibly acting to compensate for enhanced LTP in the Apoer2$^{\Delta 16+19}$ or even compensating for loss of Reelin influence in the Apoer2 $^{\Delta 16\Delta 19}$ neurons [53, 80, 86, 89].

Degradation of the ECM enhances the formation of immature filopodial spines with impaired potentiation [23], a deficit reversed by inhibiting small conductance Ca^{2+}-activated K^{+}-channels in a ROCK1-dependent manner. ROCK1 is a Rho-associated protein kinase required for cytoskeleton remodeling [64]. Within the minimal synaptic network, ROCK1 was the singular translating transcript significantly altered in Apoer2^{cKO} and cleavage-deficient mice,however, it was only up-regulated in the Apoer2 $^{\Delta 16+19}$ mouse line – the line with enhanced LTP without stimulation by Reelin. This could suggest upregulation of Apoer2 exon 19 specifically at the synapse induces ROCK1 translation leading to increased LTP. We also found reduced ribosome-association of KCNN2 transcripts, a small conductance Ca^{2+}-activated K^{+}-channel, in the Apoer2^{cKO} and the Apoer2$^{\Delta 16\Delta 19}$ lines only. KCNN2 reduces excitability leading to reduced LTP. Interestingly, synaptic activity activates the ubiquitin ligase, UBE3A, leading to KCNN2 ubiquitination [79]. UBE3A is also down-regulated in the Apoer2^{cKO} and the Apoer2 $^{\Delta 16\Delta 19}$ lines only. When potentiating input enters the synapse, UBE3A ubiquitinates KCNN2 thus reducing its hyperpolarizing input. Both are down-regulated in the Apoer2^{cKO} and Apoer2 $^{\Delta 16\Delta 19}$, while ROCK1 translating transcripts are elevated in only Apoer2$^{\Delta 16+19}$. Interestingly, loss of UBE3A is the causative factor in Angelman's syndrome, a neurodevelopmental disorder resulting in mental retardation and coordination (Madaan and Mendez, 2021).

Altered translating transcripts provide insight into synaptic dysfunction in Apoer2 KI models

While transcripts associated with overarching pathways (BDNF signaling, ion channel activity, focal adhesion,

ECM, synapse organization, nervous system development, and Fragile X Syndrome) have already been discussed, it is key to understand how several of these transcript changes may alter synaptic transmission and plasticity. For this discussion, we will only include transcripts that were significantly dysregulated in at least one genotype and rescued with both Apoer2-ICDs, thus demonstrating sufficiency of the Apoer2-ICD to regulate these translating transcripts. In Apoer2$^{\Delta16+19}$ cells, expression of *Prkcb* is decreased. Pkcrb has been shown to increase the abundance of the readily releasable pool, increasing baseline synaptic transmission [13]. This correlates with Apoer2$^{\Delta16+19}$ demonstrating decreased hippocampal output when compared to Apoer2 WT mice [86]. Further, Apoer2$^{\Delta16+19}$ mice have decreased levels of translating *Slc17a3* transcripts. *Slc17a3* codes for VGlut3, and VGlut3 KO mice demonstrated decreased mIPSC frequency and an increased threshold for LTD [27]. Apoer2$^{\Delta16+19}$ mice also demonstrated decreased translating transcripts of both *Syn1* and *Syn2*. Knockout of either synapsin gene leads to decreased post-tetanic potentiation, a form of short term-potentiation, further demonstrating Apoer2-dependent dysregulation of synaptic transmission and plasticity [71, 83]. LTP facilitation by Reelin is increased in Apoer2$^{\Delta16+19}$ mice [86], consistent with a compensatory downregulation of synapsins in the presence of an overabundance of the exon 19-encoded insert at the synapse. Meanwhile, translating *Syn1* levels are commensurately increased in Apoer2$^{\Delta16\Delta19}$ mice, providing a rationale for the phenotypic variation between Apoer2 KI mouse models. Translating transcripts of both *Lgi1* and *Adam23* are increased in Apoer2$^{\Delta16+19}$ mice. Lgi1 and possibly Adam23 work to modulate $K_v1.1$ levels and subsequently neuronal excitability while Lgi1 KO neurons also demonstrated decreased AMPA receptor currents [28]. Lastly, both Apoer2 KI models demonstrated increased levels of either translating *Rab8a* or *Rab8b*. The protein products of these transcripts are both implicated in transporting GluA1 subunits to post-synaptic spines during both receptor homeostasis and LTP [32]. This is not an exhaustive list of all synaptic genes dysregulated in cleavage-resistant Apoer2 KI models, but it demonstrates how altered translating transcripts in Apoer2$^{\Delta16\pm19}$ mice cover a vast swath of synaptic functions including membrane potential homeostasis (*Lgi1* and *Adam23*), baseline synaptic transmission (*Pkcrb* and *Slc17a3*), short term synaptic plasticity (*Syn1* and *Syn2*), LTD (*Slc17a3*), and LTP (*Rab8*). Further, by demonstrating how reintroduction of the soluble Apoer2-ICD rescues all of these transcripts, we highlight the importance of Apoer2-ICD cleavage on synaptic transmission and plasticity.

Disease implications

Our data reveal Apoer2 as a potent modulator of AD risk genes (Fig. 7A). The majority of these are known to regulate APP processing and Aβ/tau pathology. The Apoer2-ICD[+19] specifically down-regulated ribosomal association of APP transcripts in the Apoer2$^{\Delta16+19}$ hippocampi. In Apoer2^{cKO} and cleavage-deficient lines, at least one member of the γ-secretase complex was also down-regulated after expression of one of the Apoer2-ICDs. In Apoer2^{cKO} and cleavage-deficient lines, the cytoskeletal regulator CD2AP is down-regulated, and the Apoer2-ICD primarily rescues CD2AP levels in the Apoer2^{cKO} mice (and to a lesser extent in the Apoer2$^{\Delta16\Delta19}$ mice). CD2AP overexpression shunts APP from early endosomes towards lysosomal degradation [31]. The AD risk gene FERMT2 also regulates APP whereby silencing or overexpression of FERMT2 results in increased or decreased surface levels of mature APP, respectively, leading to respective changes in secreted amyloid-β [9]. In our analysis, only Apoer2$^{\Delta16+19}$ mice demonstrated decreased translating Fermt2 transcripts, an effect partially corrected by addition of the Apoer2-ICD[Δ19]. Together, these findings suggest Apoer2 and its alternative splicing influences APP homeostasis through several independent mechanisms.

Another AD risk gene, PTK2B, which encodes the Pyk2 protein, is also down-regulated in all Apoer2-ICD lacking mouse lines. Pyk2 has been implicated in the synaptic toxicity of amyloid-β oligomers in mice as well as suppressing tau toxicity in *Drosophila* [52]. Finally, we also found that overexpression of either Apoer2-ICD in Apoer2^{WT} mice increased the translating transcripts of the homolog of the AD risk gene BIN1. Decreased expression of BIN1 led to suppression of Tau-mediated neurotoxicity [10]. This suggests Apoer2 and its ICD indirectly influence both amyloid β and tau toxicity by altering the translating transcripts of known amyloid β and tau interactors.

Alongside AD, Reelin is implicated in several neuropsychiatric and neurodegenerative diseases, such as autism, schizophrenia, bipolar disorder, and major depression (reviewed in [8, 18, 21, 29, 47, 50, 51]). Despite different pathologies, reduced Reelin function is a common factor in each disorder [33, 37, 40]. With the lack or overexpression of the Apoer2-ICD, we find a similar disease imprint as its ligand, Reelin. One key transcript that presents in our dataset, GSK3β, is a central hub in AD and schizophrenia. GSK3β is upregulated in both cleavage-resistant Apoer2 mouse models, an effect rescued by either Apoer2-ICD (Fig. 5, 6). Reelin signaling through Apoer2 and Vldlr inhibits GSK3β, which when active, phosphorylates tau [44]. This inhibition prevents hyperphosphorylation of tau, an event known to result in tau

aggregation and formation of the hallmark AD neurofibrillary tangles. This suggests Reelin not only reduces the activity of GSK3β by signaling through Apoer2, but possibly also by reducing the number of translating transcripts of this constitutively active kinase via ligand-binding induced cleavage of Apoer2.

Another synaptic hub protein that is implicated in AD and schizophrenia, β-catenin (CTNNB1), is a core participant in Wnt-signaling, and the number of translating CTNNB1 transcripts is down-regulated in the Apoer2^{cKO} (Fig. 4). The Wnt-signaling pathway, much like Reelin signaling, regulates brain development, synapse formation and synapse function [41]. Two other members of the low-density lipoprotein receptor family, LRP5 and LRP6, are central to Wnt signaling. Both are co-receptors with the Frizzled receptor (FZD) for Wnt ligands, resulting in reduced degradation of β-catenin [66, 67]. Additionally, neuronal knockout of Lrp6 in mice causes deficits in synaptic integrity and memory formation. When crossed with the APP/PS1 line, Lrp6 KO mice demonstrated enhanced Aβ production leading to inhibition of Wnt signaling, a finding also seen in Alzheimer brains [55]. Interestingly, clozapine reduced β-catenin and TCF-4 (encoded by TCF7L2), an effect mediated through down-regulation of TNIK (Traf2- and Nck-interacting kinase) [90]. TNIK is up-regulated by either Apoer2-ICD (Fig. 3), which provides another mechanism by which reduced Reelin signaling could impart risk for psychosis. These experiments reveal a landscape of critical synaptic proteins altered in the absence of the Apoer2-ICD. Further exploration is required to understand how these changes affect the synaptic environment,however, our study, together with the protective nature of a Reelin gain-of-function mutation [56], demonstrates the importance of Reelin/Apoer2 signaling for AD pathogenesis.

Limitations of the study

A major limitation of this study is the inability to quantify the proteomic consequences of the Apoer2-ICD. Because we are reintroducing the Apoer2-ICD through viral infection, only a subset of cells (~10%) will express our construct. Therefore, the signal-to-noise ratio of bulk RNA-Seq or proteomics would be too low to ascertain Apoer2-ICD-dependent changes *in vivo*. For this reason, we utilized our Cre-dependent TRAP protocol to isolate mRNA strictly from lentivirus-infected - and thus ICD expressing - cells. While this approach cannot reveal differential protein expression in the infected cells, the specificity and sensitivity of the technique allowed us to detect changes of ribosome-primed transcripts secondary to the presence or absence of Apoer2-ICD.

Further, while our approach does not specifically differentiate between hippocampal cell-types, it does reflect the physiological context of the hippocampus where Apoer2 is expressed in all cells. By complementing our data analysis with single cell sequencing databases, we were nonetheless able to ascribe the majority of the mRNA expression changes to neurons [45] (Figure S6A), demonstrating the effect of Apoer2-ICD expression primarily on hippocampal neurons. Likewise, by analyzing the levels of genetic markers for various cell types (astrocytes, oligodendrocytes, microglia, epithelial cells, and neurons), we were able to ascertain that the majority of the cells isolated for our TRAP-Seq analysis were neuronal (Figure S6B).

Abbreviations

ABCA7	ATP Binding Cassette Subfamily A Member 7
ABI2	Abl Interactor 2
ABL1	ABL proto-oncogene 1
ACE	Angiotensin I Converting Enzyme
ACTA2	Actin Alpha 2, Smooth Muscle
ACTC1	Actin Alpha Cardiac Muscle 1
ACTG1	Actin Gamma 1
ACTN1	Actinin Alpha 1
ACTR3	Actin Related Protein 3
AD	Alzheimer's disease
ADAM23	ADAM Metallopeptidase Domain 23
ADGRB3	Adhesion G Protein-Coupled Receptor B3
ADRA1A	Adrenoceptor Alpha 1A
AKAP12	A-Kinase Anchoring Protein 12
AMPA	α-Amino-3-hydroxy-5-methyl-4-isoxazolepropionic acid
ANO6	Anoctamin 6
AP1G1	AP-1 complex subunit gamma-1
APH1B	Aph-1 Homolog B, Gamma-Secretase Subunit
APOE	Apolipoprotein E
APOER2	Apolipoprotein E receptor 2
APP	Amyloid precursor protein
ARC	Activity Regulated Cytoskeleton Associated Protein
ARHGAP18	Rho GTPase Activating Protein 18
ARHGAP44	Rho GTPase Activating Protein 44
ARHGEF2	Rho/Rac Guanine Nucleotide Exchange Factor 2
ARID1B	AT-Rich Interaction Domain 1B
ASAP1	ArfGAP With SH3 Domain, Ankyrin Repeat And PH Domain 1
ATP6V1D	ATPase H+ Transporting V1 Subunit D
ATP6V1E1	ATPase H+ Transporting V1 Subunit E1
AURKA	Aurora Kinase A
Aβ	Amyloid beta
BDNF	Brain-derived neurotrophic factor
BIN1	Bridging Integrator 1
BRWD1	Bromodomain And WD Repeat Domain Containing 1
CACNG5	Calcium Voltage-Gated Channel Auxiliary Subunit Gamma 5
CASP3	Caspase 3
CBL	CBL Proto-Oncogene
CD2AP	CD2 Associated Protein
CDC42	Cell Division Cycle 42
CDH6	Cadherin 6
CDK5	Cyclin-dependent kinase 5
CDKL5	Cyclin-dependent kinase-like 5
COL1A2	Collagen Type I Alpha 2 Chain
COPG2	COPI Coat Complex Subunit Gamma 2
COX7A2L	Cytochrome C Oxidase Subunit 7A2 Like
CPEB1	Cytoplasmic polyadenylation element-binding protein 1
CR1	Complement C3b/C4b Receptor 1 (Knops Blood Group)
CRK	CRK Proto-Oncogene, Adaptor Protein
CTNNB1	Catenin Beta 1
CTSB	Cathepsin B
CTSH	Cathepsin H

DBYSL2	Dihydropyrimidinase Like 2
DLG1	Discs Large MAGUK Scaffold Protein 1
DLG5	Discs Large MAGUK Scaffold Protein 5
DNM1	Dynamin 1
DPYSL2	Dihydropyrimidinase Like 2
DRD1	Dopamine Receptor D1
DRD2	Dopamine Receptor D2
DSP	Desmoplakin
DYNLRB2	Dynein light chain roadblock-type 2
ECD	Extracellular domain
ECM	Extracellular matrix
EEF2K	Eukaryotic Elongation Factor 2 Kinase
EFNA5	Ephrin A5
EIF2B2	Eukaryotic initiation factor-2B
EIF2S1	Eukaryotic Translation Initiation Factor 2 Subunit Alpha
EIF4E	Eukaryotic translation initiation factor 4E
EIF4G3	Eukaryotic Translation Initiation Factor 4 Gamma 3
ELAVL4	ELAV Like RNA Binding Protein 4
ENPP2	Ectonucleotide Pyrophosphatase/Phosphodiesterase 2
ERBB2	Receptor tyrosine-protein kinase erbB-2
FERMT2	FERM Domain Containing Kindlin 2
FYN	Fyn Proto-Oncogene, Src Family Tyrosine Kinase
FZD	Frizzled
FZD2	Frizzled Class Receptor 2
FZD4	Frizzled Class Receptor 4
FZD8	Frizzled Class Receptor 8
GABA	Gamma-aminobutyric acid
GFP	Green fluorescent protein
GLRA2	Glycine receptor subunit alpha-2
GLUA1	Glutamate Ionotropic Receptor AMPA Type Subunit 1
GRIN2D	Glutamate Ionotropic Receptor NMDA Type Subunit 2D
GRN	Progranulin
GSEA	Gene Set Enrichment Analysis
GSK3B	Glycogen Synthase Kinase 3 Beta
GSTM1	Glutathione S-Transferase Mu 1
HAGH	Hydroxyacylglutathione hydrolase
HDAC1	Histone deacetylase 1
HNRNPK	Heterogeneous Nuclear Ribonucleoprotein K
HNRNPL	Heterogeneous Nuclear Ribonucleoprotein L
HTR1A	5-Hydroxytryptamine Receptor 1A
HTR1F	5-Hydroxytryptamine Receptor 1F
ICD	Intracellular domain
IRES	Internal ribosome entry site
ITGA3	Integrin Subunit Alpha 3
ITGB1	Integrin Subunit Beta 1
ITGB3	Integrin Subunit Beta 3
ITGB5	Integrin Subunit Beta 5
JAG1	Jagged Canonical Notch Ligand 1
KBTBD12	Kelch Repeat And BTB Domain Containing 12
KCNN2	Potassium Calcium-Activated Channel Subfamily N Member 2
KDM3A	Lysine Demethylase 3A
KDM4B	Lysine-specific demethylase 4B
KIF5A	Kinesin family member 5A
LAMA4	Laminin Subunit Alpha 4
LGI1	Leucine-rich glioma-inactivated 1
LOAD	Late-onset Alzheimer's disease
LPAR1	Lysophosphatidic Acid Receptor 1
LRP1	Low-density lipoprotein receptor related protein 1
LRP3	Low-density lipoprotein receptor-related protein 3
LRP5	LDL Receptor Related Protein 5
LRP6	LDL Receptor Related Protein 6
LRP8	Low-density lipoprotein receptor related protein 8
LTP	Long-term potentiation
LZTS1	Leucine Zipper Tumor Suppressor 1
MAP2K2	Mitogen-Activated Protein Kinase Kinase 2
MAPK3	Mitogen-Activated Protein Kinase 3
MAPK8	Mitogen-Activated Protein Kinase 8
MARCKS	Myristoylated alanine-rich C-kinase substrate
mIPSC	Miniature inhibitory postsynaptic currents
mTOR	Mammalian target of rapamycin
NAPB	NSF Attachment Protein Beta
NCOA2	Nuclear Receptor Coactivator 2
ND6	NADH dehydrogenase 6
NDEL1	NudE Neurodevelopment Protein 1 Like 1
NEDD4	NEDD4 E3 Ubiquitin Protein Ligase
NF1	Neurofibromatosis type 1
NGFR	Nerve Growth Factor Receptor
NOS1	Nitric oxide synthase 1
OPHN1	Oligophrenin 1
OPRK1	Opioid Receptor Kappa 1
P2RY1	Purinergic Receptor P2Y1
PI3K	Phosphoinositide 3-kinase
PICK1	Protein Interacting With PRKCA 1
PIK3R1	Phosphoinositide-3-Kinase Regulatory Subunit 1
PLCG1	Phospholipase C gamma 1
PLCG2	Phospholipase C Gamma 2
PPFI2A	PTPRF Interacting Protein Alpha 2
PRKCB	Protein kinase C beta type
PRKCD	Protein kinase C delta type
PS1	Presenilin-1
PSD-95	Post-synaptic density protein 95
PSEN2	Presenilin 2
PSENEN	Presenilin Enhancer
PTEN	Phosphatase and tensin homolog
PTK2B	Protein Tyrosine Kinase 2 Beta
PTPRN2	Protein Tyrosine Phosphatase Receptor Type N2
PUM2	Pumilio RNA Binding Family Member 2
PYK2	Protein Tyrosin Kinase 2
RAB11A	RAB11A, Member RAS Oncogene Family
RAB3B	RAB3B, Member RAS Oncogene Family
RAB3GAP2	RAB3 GTPase Activating Non-Catalytic Protein Subunit 2
RAB8A	RAB8A, Member RAS Oncogene Family
RAB8B	RAB8B, Member RAS Oncogene Family
RAC1	Rac Family Small GTPase 1
RALGAPA2	Ral GTPase Activating Protein Catalytic Subunit Alpha 2
RAP1B	RAP1B, Member Of RAS Oncogene Family
RAPGEF1	Rap Guanine Nucleotide Exchange Factor 1
RAPSN	Receptor Associated Protein Of The Synapse
RASAL2	RAS Protein Activator Like 2
RASD2	RASD Family Member 2
RCC2	Regulator Of Chromosome Condensation 2
RGS7BP	Regulator Of G Protein Signaling 7 Binding Protein
ROCK1	Rho associated coiled-coil containing protein kinase 1
ROCK2	Rho Associated Coiled-Coil Containing Protein Kinase 2
ROR2	Receptor Tyrosine Kinase Like Orphan Receptor 2
RPTOR	Regulatory Associated Protein Of MTOR Complex 1
S100B	S100 Calcium Binding Protein B
SCN10A	Sodium Voltage-Gated Channel Alpha Subunit 10
SCRN1	Secernin 1
SDCBP	Syndecan Binding Protein
SETD2	SET domain containing 2
SHISA9	Shisa Family Member 9
SLC17A3	Solute Carrier Family 17 Member 3
SLC1A1	Solute Carrier Family 1 Member 1
SLC39A9	Solute Carrier Family 39 Member 9
SLC6A11	Solute Carrier Family 6 Member 11
SLITRK3	SLIT And NTRK Like Family Member 3
SLITRK4	SLIT And NTRK Like Family Member 4
SMAD5	SMAD Family Member 5
SORL1	Sortilin Related Receptor 1
SRC	SRC Proto-Oncogene, Non-Receptor Tyrosine Kinase
STX6	Syntaxin 6
SV2B	Synaptic vesicle glycoprotein 2B
SVOP	SV2 Related Protein
SYN1	Synapsin I
SYN2	Synapsin 2
SYP	Synaptophysin
SYT12	Synaptotagmin 12
TANC1	Tetratricopeptide Repeat, Ankyrin Repeat And Coiled-Coil Containing 1
TCF7L2	Transcription factor 7-like 2 (T-cell specific, HMG-box)
TFAP2B	Transcription Factor AP-2 Beta

TNC	Tenascin C
TNIK	TRAF2 And NCK Interacting Kinase
TRAP	Translating-ribosome affinity purification
TRN	Tenascin R
TRPM1	Transient Receptor Potential Cation Channel Subfamily M Member 1
TUBB2B	Tubulin Beta 2B Class IIb
UBE3A	Ubiquitin Protein Ligase E3A
UBR5	Ubiquitin-protein ligase N-recognin 5
UNC13B	Unc-13 Homolog B
VAMP3	Vesicle Associated Membrane Protein 3
VAPA	VAMP Associated Protein A
VGLUT3	Vesicular Glutamate Transporter 3
VLDLR	Very low-density lipoprotein receptor
VPS35	Vacuolar protein sorting ortholog 35
WNT5A	Wnt Family Member 5A
YES1	YES Proto-Oncogene 1, Src Family Tyrosine Kinase
ZNF644	Zinc Finger Protein 644

Supplementary Information

The online version contains supplementary material available at https://doi.org/10.1186/s13024-023-00652-1.

Additional file 1: Figure S1. Regulation of Apoer2-ICD promoter-binding and effects of Apoer2-ICD mutations on *Reln*-promoter binding *in vitro*. **Figure S2.** Volcano plots of key TRAP-Seq comparisons. **Figure S3.** Transcription factors similarly regulated in Apoer2^{cKO} and cleavage-deficient hippocampi. **Figure S4.** Overlapping overall transcript changes by genotype. **Figure S5.** Functional enrichments for all conditions by genotype. **Figure S6.** Majority of altered transcripts are specifically neuronal.

Additional file 2: Table S1. All differentially regulated translating transcripts in Apoer2^{WT}. **Table S2.** All differentially regulated translating transcripts in Apoer2^{cKO}. **Table S3.** All differentially regulated translating transcripts in Apoer2$^{\Delta16+19}$. **Table S4.** All differentially regulated translating transcripts in Apoer2$^{\Delta16\Delta19}$. **Table S5.** Similar basal translatome changes across Apoer2 cKO/KI samples and functional enrichment categories with associated transcripts in Apoer2 cKO/KI samples compared to Apoer2 WT in Figure 2D-E. **Table S6-S9.** Functional enrichments of basal and Apoer2-ICD-induced translating transcript differences in the Apoer2^{WT} (Table S6), Apoer2^{cKO} (Table S7), Apoer2$^{\Delta16+19}$(Table S8), and Apoer2$^{\Delta16\Delta19}$ (Table S9) samples. **Table S10.** Raw data for log_2FC and p-values for all transcripts isolated from mouse hippocampi with and without reintroduction of Apoer2-ICD. **Table S11.** Sequences used in constructs (from 3'à 5').

Acknowledgements
We thank Tamara Terrones, Patricia Strackbein, Rebekah Hewitt, Anna E. Alexander, Isaac Rocha for technical assistance. We thank Theresa Pohlkamp, and Anna E. Alexander for critical comments.

Authors' contributions
C.R.W. and J.H. conceptualized the project, methodology, and acquired funding. E.H. cloned all constructs and performed all luciferase assays. G.C.W. and C.R.W. performed all experiments, analysis, and interpretation. C.R.W. and G.C.W designed all figures and wrote the manuscript, K.K., M.S.D., C.H.W., and J.H. reviewed and edited the manuscript. J.H. supervised the project.

Funding
This work was supported by the National Institutes of Health National Institute on Aging (NIA) RF1 AG053391; National Heart, Lung and Blood Institute (NHLBI) R37 HL063762; National Institute of Neurological Disorders and Stroke (NINDS) and NIA Grants R01 NS093382 and NS108115; BrightFocus Foundation Grants A20135245 and A2016396S; Harrington Discovery Institute; Blue Field Project to Cure Frontotemporal Dementia to J.H. K.K. received funding from the German Research Foundation (KU 4036/1-1).

Availability of data and materials
Primary data have been uploaded to the following address. https://dataverse.tdl.org/dataverse/Apoer2-ICD_translatome.

Further information and requests for resources, reagents, and data should be directed to and will be fulfilled by the lead contact: Dr. Catherine Wasser. (catherine.wasser@utsouthwestern.edu).

Declarations

Ethics approval and consent to participate
Not applicable.

Consent for publication
Not applicable.

Competing interests
The authors declare no competing interests.
Joachim Herz is a cofounder of Reelin Therapeutics.

Author details
[1]Department of Molecular Genetics, UT Southwestern, 5323 Harry Hines Blvd, Dallas, TX 75390-9046, USA. [2]Center for Translational Neurodegeneration Research, Department of Molecular Genetics, UT Southwestern, 5323 Harry Hines Blvd, Dallas, TX, USA. [3]Department of Neuroscience, UT Southwestern, Dallas, TX, USA. [4]Neurology and Neurotherapeutics, University of Texas Southwestern Medical Center, Dallas, TX, USA.

Received: 13 June 2023 Accepted: 24 August 2023
Published online: 19 September 2023

References

1. Balmaceda V, Cuchillo-Ibanez I, Pujadas L, Garcia-Ayllon MS, Saura CA, Nimpf J, Soriano E, Saez-Valero J. ApoER2 processing by presenilin-1 modulates reelin expression. FASEB J. 2014;28:1543–54.
2. Beffert U, Weeber EJ, Durudas A, Qiu S, Masiulis I, Sweatt JD, Li WP, Adelmann G, Frotscher M, Hammer RE, et al. Modulation of synaptic plasticity and memory by Reelin involves differential splicing of the lipoprotein receptor Apoer2. Neuron. 2005;47(4):567–79. https://doi.org/10.1016/j.neuron.2005.07.007.
3. Bellenguez C, Kucukali F, Jansen IE, Kleineidam L, Moreno-Grau S, Amin N, et al. New insights into the genetic etiology of Alzheimer's disease and related dementias. Nat Genet. 2022;54(4):412–36. https://doi.org/10.1038/s41588-022-01024-z.
4. Bindea G, Galon J, Mlecnik B. CluePedia Cytoscape plugin: pathway insights using integrated experimental and in silico data. Bioinformatics. 2013;29:661–3.
5. Bindea G, Mlecnik B, Hackl H, Charoentong P, Tosolini M, Kirilovsky A, Fridman WH, Pages F, Trajanoski Z, Galon J. ClueGO: a Cytoscape plug-in to decipher functionally grouped gene ontology and pathway annotation networks. Bioinformatics. 2009;25:1091–3.
6. Botella-Lopez A, Burgaya F, Gavin R, Garcia-Ayllon MS, Gomez-Tortosa E, Pena-Casanova J, Urena JM, Del Rio JA, Blesa R, Soriano E, et al. Reelin expression and glycosylation patterns are altered in Alzheimer's disease. Proc Natl Acad Sci U S A. 2006;103:5573–8.
7. Bracher-Smith M, Leonenko G, Baker E, Crawford K, Graham AC, Salih DA, Howell BW, Hardy J, Escott-Price V. Whole genome analysis in APOE4 homozygotes identifies the DAB1-RELN pathway in Alzheimer's disease pathogenesis. Neurobiol Aging. 2022;119:67–76. https://doi.org/10.1016/j.neurobiolaging.2022.07.009.
8. Caruncho HJ, Dopeso-Reyes IG, Loza MI, Rodriguez MA. A GABA, reelin, and the neurodevelopmental hypothesis of schizophrenia. Crit Rev Neurobiol. 2004;16:25–32.
9. Chapuis J, Flaig A, Grenier-Boley B, Eysert F, Pottiez V, Deloison G, Vandeputte A, Ayral AM, Mendes T, Desai S, Goate AM, Kauwe JSK, Leroux F, Herledan A, Demiautte F, Bauer C, Checler F, Petersen RC, Blennow K, Zetterberg H, ..., ADGC, Alzheimer's Disease Neuroimaging Initiative. Genome-wide, high-content siRNA screening identifies the Alzheimer's genetic risk factor FERMT2 as a major modulator of APP metabolism. Acta Neuropathol. 2017;133(6):955–66. https://doi.org/10.1007/s00401-016-1652-z.
10. Chapuis J, Hansmannel F, Gistelinck M, Mounier A, Van Cauwenberghe C, Kolen KV, Geller F, Sottejeau Y, Harold D, Dourlen P, Grenier-Boley B,

Kamatani Y, Delepine B, Demiautte F, Zelenika D, Zommer N, Hamdane M, Bellenguez C, Dartigues JF, Hauw JJ, ..., GERAD consortium. Increased expression of BIN1 mediates Alzheimer genetic risk by modulating tau pathology. Mol Psychiatry. 2013;18(11):1225–34. https://doi.org/10.1038/mp.2013.1.
11. Chen J, Bardes EE, Aronow BJ, Jegga AG. ToppGene Suite for gene list enrichment analysis and candidate gene prioritization. Nucleic Acids Res. 2009;37:W305–311.
12. Chin J, Massaro CM, Palop JJ, Thwin MT, Yu GQ, Bien-Ly N, Bender A, Mucke L. Reelin depletion in the entorhinal cortex of human amyloid precursor protein transgenic mice and humans with Alzheimer's disease. J Neurosci. 2007;27:2727–33.
13. Chu Y, Fioravante D, Leitges M, Regehr WG. Calcium-dependent PKC isoforms have specialized roles in short-term synaptic plasticity. Neuron. 2014;82(4):859–71.
14. Clarke DJB, Jeon M, Stein DJ, Moiseyev N, Kropiwnicki E, Dai C, Xie Z, Wojciechowicz ML, Litz S, Hom J, et al. Appyters: Turning Jupyter Notebooks into data-driven web apps. Patterns (N Y). 2021;2:100213.
15. Colombo M, Karousis ED, Bourquin J, Bruggmann R, Muhlemann O. Transcriptome-wide identification of NMD-targeted human mRNAs reveals extensive redundancy between SMG6- and SMG7-mediated degradation pathways. RNA. 2017;23:189–201.
16. Consortium, E.P. An integrated encyclopedia of DNA elements in the human genome. Nature. 2012;489:57–74.
17. Corder EH, Saunders AM, Strittmatter WJ, Schmechel DE, Gaskell PC, Small GW, Roses AD, Haines JL, Pericak-Vance MA. Gene dose of apolipoprotein E type 4 allele and the risk of Alzheimer's disease in late onset families. Science. 1993;261:921–3.
18. Costa E, Davis J, Grayson DR, Guidotti A, Pappas GD, Pesold C. Dendritic spine hypoplasticity and downregulation of reelin and GABAergic tone in schizophrenia vulnerability. Neurobiol Dis. 2001;8:723–42.
19. Cuchillo-Ibanez I, Lennol MP, Escamilla S, Mata-Balaguer T, Valverde-Vozmediano L, Lopez-Font I, Ferrer I, Saez-Valero J. The apolipoprotein receptor LRP3 compromises APP levels. Alzheimers Res Ther. 2021;13:181.
20. da Huang W, Sherman BT, Lempicki RA. Systematic and integrative analysis of large gene lists using DAVID bioinformatics resources. Nat Protoc. 2009;4:44–57.
21. D'Arcangelo G. Reelin mouse mutants as models of cortical development disorders. Epilepsy Behav. 2006;8:81–90.
22. D'Arcangelo G, Miao GG, Chen SC, Soares HD, Morgan JI, Curran T. A protein related to extracellular matrix proteins deleted in the mouse mutant reeler. Nature. 1995;374:719–23.
23. Dembitskaya Y, Gavrilov N, Kraev I, Doronin M, Tang Y, Li L, Semyanov A. Attenuation of the extracellular matrix increases the number of synapses but suppresses synaptic plasticity through upregulation of SK channels. Cell Calcium. 2021;96:102406.
24. Dobin A, Davis CA, Schlesinger F, Drenkow J, Zaleski C, Jha S, Batut P, Chaisson M, Gingeras TR. STAR: ultrafast universal RNA-seq aligner. Bioinformatics. 2013;29:15–21.
25. Dong E, Caruncho H, Liu WS, Smalheiser NR, Grayson DR, Costa E, Guidotti A. A reelin-integrin receptor interaction regulates Arc mRNA translation in synaptoneurosomes. Proc Natl Acad Sci U S A. 2003;100:5479–84.
26. Dumanis SB, Cha HJ, Song JM, Trotter JH, Spitzer M, Lee JY, Weeber EJ, Turner RS, Pak DT, Rebeck GW, et al. ApoE receptor 2 regulates synapse and dendritic spine formation. PLoS ONE. 2011;6:e17203.
27. Fasano C, Rocchetti J, Pietrajtis K, Zander JF, Manseau F, Sakae DY, Marcus-Sells M, Ramet L, Morel LJ, Carrel D, Dumas S, Bolte S, Bernard V, Vigneault E, Goutagny R, Ahnert-Hilger G, Giros B, Daumas S, Williams S, El Mestikawy S. Regulation of the Hippocampal Network by VGLUT3-Positive CCK- GABAergic Basket Cells. Front Cell Neurosci. 2017;11:140.
28. Fels E, Muñiz-Castrillo S, Vogrig A, Joubert B, Honnorat J, Pascual O. Role of LGI1 protein in synaptic transmission: From physiology to pathology. Neurobiol Dis. 2021;160:105537.
29. Folsom TD, Fatemi SH. The involvement of Reelin in neurodevelopmental disorders. Neuropharmacology. 2013;68:122–35.
30. Förster E, Bock HH, Herz J, Chai X, Frotscher M, Zhao S. Emerging topics in Reelin function. Eur J Neurosci. 2010;31(9):1511–518. https://doi.org/10.1111/j.1460-9568.2010.07222.x.
31. Furusawa K, Takasugi T, Chiu YW, Hori Y, Tomita T, Fukuda M, Hisanaga SI. CD2-associated protein (CD2AP) overexpression accelerates amyloid precursor protein (APP) transfer from early endosomes to the lysosomal degradation pathway. J Biol Chem. 2019;294(28):10886–99.
32. Gerges NZ, Backos DS, Esteban JA. Local control of AMPA receptor trafficking at the postsynaptic terminal by a small GTPase of the Rab family. J Biol Chem. 2004;279(42):43870–8.
33. Guidotti A, Auta J, Davis JM, Di-Giorgi-Gerevini V, Dwivedi Y, Grayson DR, Impagnatiello F, Pandey G, Pesold C, Sharma R, et al. Decrease in reelin and glutamic acid decarboxylase67 (GAD67) expression in schizophrenia and bipolar disorder: a postmortem brain study. Arch Gen Psychiatry. 2000;57:1061–9.
34. Heiman M, Kulicke R, Fenster RJ, Greengard P, Heintz N. Cell type-specific mRNA purification by translating ribosome affinity purification (TRAP). Nat Protoc. 2014;9:1282–91.
35. Heiman M, Schaefer A, Gong S, Peterson JD, Day M, Ramsey KE, Suarez-Farinas M, Schwarz C, Stephan DA, Surmeier DJ, et al. A translational profiling approach for the molecular characterization of CNS cell types. Cell. 2008;135:738–48.
36. Helbecque N, Cottel D, Amouyel P. Low-density lipoprotein receptor-related protein 8 gene polymorphisms and dementia. Neurobiol Aging. 2009;30:266–71.
37. Herring A, Donath A, Steiner KM, Widera MP, Hamzehian S, Kanakis D, Kolble K, ElAli A, Hermann DM, Paulus W, et al. Reelin depletion is an early phenomenon of Alzheimer's pathology. J Alzheimers Dis. 2012;30:963–79.
38. Herz J, Bock HH. Lipoprotein receptors in the nervous system. Annu Rev Biochem. 2002;71:405–34.
39. Hinrich AJ, Jodelka FM, Chang JL, Brutman D, Bruno AM, Briggs CA, James BD, Stutzmann GE, Bennett DA, Miller SA, et al. Therapeutic correction of ApoER2 splicing in Alzheimer's disease mice using antisense oligonucleotides. EMBO Mol Med. 2016;8:328–45.
40. Impagnatiello F, Guidotti AR, Pesold C, Dwivedi Y, Caruncho H, Pisu MG, Uzunov DP, Smalheiser NR, Davis JM, Pandey GN, et al. A decrease of reelin expression as a putative vulnerability factor in schizophrenia. Proc Natl Acad Sci U S A. 1998;95:15718–23.
41. Inestrosa NC, Montecinos-Oliva C, Fuenzalida M. Wnt signaling: role in Alzheimer disease and schizophrenia. J Neuroimmune Pharmacol. 2012;7:788–807.
42. Jaudon F, Thalhammer A, Cingolani LA. Integrin adhesion in brain assembly: From molecular structure to neuropsychiatric disorders. Eur J Neurosci. 2021;53:3831–50.
43. Jiang W, Hua R, Wei M, Li C, Qiu Z, Yang X, Zhang C. An optimized method for high-titer lentivirus preparations without ultracentrifugation. Sci Rep. 2015;5:13875.
44. Jossin Y, Goffinet AM. Reelin signals through phosphatidylinositol 3-kinase and Akt to control cortical development and through mTor to regulate dendritic growth. Mol Cell Biol. 2007;27:7113–24.
45. Karlsson M, Zhang C, Mear L, Zhong W, Digre A, Katona B, Sjostedt E, Butler L, Odeberg J, Dusart P, et al. A single-cell type transcriptomics map of human tissues. Sci Adv. 2021;7(31). https://doi.org/10.1126/sciadv.abh2169.
46. Kamboh MI. Genomics and Functional Genomics of Alzheimer's Disease. Neurotherapeutics. 2022;19:152–72.
47. Knuesel I. Reelin-mediated signaling in neuropsychiatric and neurodegenerative diseases. Prog Neurobiol. 2010;91:257–74.
48. Koch S, Strasser V, Hauser C, Fasching D, Brandes C, Bajari TM, Schneider WJ, Nimpf J. A secreted soluble form of ApoE receptor 2 acts as a dominant-negative receptor and inhibits Reelin signaling. EMBO J. 2002;21:5996–6004.
49. Koopmans F, van Nierop P, Andres-Alonso M, Byrnes A, Cijsouw T, Coba MP, Cornelisse LN, Farrell RJ, Goldschmidt HL, Howrigan DP, et al. SynGO: An Evidence-Based, Expert-Curated Knowledge Base for the Synapse. Neuron. 2019;103(217–234):e214.
50. Lakatosova S, Ostatnikova D. Reelin and its complex involvement in brain development and function. Int J Biochem Cell Biol. 2012;44:1501–4.
51. Lane-Donovan C, Philips GT, Wasser CR, Durakoglugil MS, Masiulis I, Upadhaya A, Pohlkamp T, Coskun C, Kotti T, Steller L, et al. Reelin protects against amyloid beta toxicity in vivo. Sci Signal. 2015;8(384):ra67.
52. Lee S, Salazar SV, Cox TO, Strittmatter SM. Pyk2 Signaling through Graf1 and RhoA GTPase Is Required for Amyloid-β Oligomer-Triggered Synapse Loss. J Neurosci. 2019;39(10):1910–29. https://doi.org/10.1523/JNEUROSCI.2983-18.2018.

53. Li J, Han W, Pelkey KA, Duan J, Mao X, Wang YX, Craig MT, Dong L, Petralia RS, McBain CJ, et al. Molecular Dissection of Neuroligin 2 and Slitrk3 Reveals an Essential Framework for GABAergic Synapse Development. Neuron. 2017;96(808–826):e808.
54. Liao Y, Smyth GK, Shi W. featureCounts: an efficient general purpose program for assigning sequence reads to genomic features. Bioinformatics. 2014;30:923–30.
55. Liu CC, Tsai CW, Deak F, Rogers J, Penuliar M, Sung YM, Maher JN, Fu Y, Li X, Xu H, et al. Deficiency in LRP6-mediated Wnt signaling contributes to synaptic abnormalities and amyloid pathology in Alzheimer's disease. Neuron. 2014;84:63–77.
56. Lopera F, Marino C, Chandrahas AS, et al. Resilience to autosomal dominant Alzheimer's disease in a Reelin-COLBOS heterozygous man. Nat Med. 2023;29:1243–52. https://doi.org/10.1038/s41591-023-02318-3.
57. Lotia S, Montojo J, Dong Y, Bader GD, Pico AR. Cytoscape app store. Bioinformatics. 2013;29:1350–1.
58. Love MI, Huber W, Anders S. Moderated estimation of fold change and dispersion for RNA-seq data with DESeq2. Genome Biol. 2014;15:550.
59. Luo Y, Hitz BC, Gabdank I, Hilton JA, Kagda MS, Lam B, Myers Z, Sud P, Jou J, Lin K, et al. New developments on the Encyclopedia of DNA Elements (ENCODE) data portal. Nucleic Acids Res. 2020;48(D1):D882–9. https://doi.org/10.1093/nar/gkz1062.
60. May P, Bock HH, Nimpf J, Herz J. Differential glycosylation regulates processing of lipoprotein receptors by gamma-secretase. J Biol Chem. 2003;278:37386–92.
61. May P, Reddy YK, Herz J. Proteolytic processing of low density lipoprotein receptor-related protein mediates regulated release of its intracellular domain. J Biol Chem. 2002;277:18736–43.
62. Mootha VK, Lindgren CM, Eriksson KF, Subramanian A, Sihag S, Lehar J, Puigserver P, Carlsson E, Ridderstrale M, Laurila E, et al. PGC-1alpha-responsive genes involved in oxidative phosphorylation are coordinately downregulated in human diabetes. Nat Genet. 2003;34:267–73.
63. Morris J, Singh JM, Eberwine JH. Transcriptome analysis of single cells. J Vis Exp. 2011;(50):e2634. https://doi.org/10.3791/2634.
64. Nakayama AY, Harms MB, Luo L. Small GTPases Rac and Rho in the maintenance of dendritic spines and branches in hippocampal pyramidal neurons. J Neurosci. 2000;20:5329–38.
65. Niu S, Yabut O, D'Arcangelo G. The Reelin signaling pathway promotes dendritic spine development in hippocampal neurons. J Neurosci. 2008;28:10339–48.
66. Nusse R, Clevers H. Wnt/beta-Catenin Signaling, Disease, and Emerging Therapeutic Modalities. Cell. 2017;169:985–99.
67. Pohlkamp T, Wasser CR, Herz J. Functional Roles of the Interaction of APP and Lipoprotein Receptors. Front Mol Neurosci. 2017;10:54.
68. Pujadas L, Rossi D, Andres R, Teixeira CM, Serra-Vidal B, Parcerisas A, Maldonado R, Giralt E, Carulla N, Soriano E. Reelin delays amyloid-beta fibril formation and rescues cognitive deficits in a model of Alzheimer's disease. Nat Commun. 2014;5:3443.
69. Qiu S, Weeber EJ. Reelin signaling facilitates maturation of CA1 glutamatergic synapses. J Neurophysiol. 2007;97:2312–21.
70. Reddy SS, Connor TE, Weeber EJ, Rebeck W. Similarities and differences in structure, expression, and functions of VLDLR and ApoER2. Mol Neurodegener. 2011;6:30.
71. Rosahl T, Spillane D, Missler M, et al. Essential functions of synapsins I and II in synaptic vesicle regulation. Nature. 1995;375:488–93.
72. Shah S, Lee SF, Tabuchi K, Hao YH, Yu C, LaPlant Q, Ball H, Dann CE 3rd, Sudhof T, Yu G. Nicastrin functions as a gamma-secretase-substrate receptor. Cell. 2005;122:435–47.
73. Sjöstedt E, Zhong W, Fagerberg L, Karlsson M, Mitsios N, Adori C, Oksvold P, Edfors F, Limiszewska A, Hikmet F, Huang J, Du Y, Lin L, Dong Z, Yang L, Liu X, Jiang H, Xu X, Wang J, Yang H, Mulder J. An atlas of the protein-coding genes in the human, pig, and mouse brain. Science (New York, N.Y.). 2020;367(6482):eaay5947. https://doi.org/10.1126/science.aay5947.
74. Stockinger W, Brandes C, Fasching D, Hermann M, Gotthardt M, Herz J, Schneider WJ, Nimpf J. The reelin receptor ApoER2 recruits JNK-interacting proteins-1 and -2. J Biol Chem. 2000;275:25625–32.
75. Strasser V, Fasching D, Hauser C, Mayer H, Bock HH, Hiesberger T, Herz J, Weeber EJ, Sweatt JD, Pramatarova A, et al. Receptor clustering is involved in Reelin signaling. Mol Cell Biol. 2004;24:1378–86.
76. Strittmatter WJ, Roses AD. Apolipoprotein E and Alzheimer's disease. Annu Rev Neurosci. 1996;19:53–77.
77. Subramanian A, Tamayo P, Mootha VK, Mukherjee S, Ebert BL, Gillette MA, Paulovich A, Pomeroy SL, Golub TR, Lander ES, et al. Gene set enrichment analysis: a knowledge-based approach for interpreting genome-wide expression profiles. Proc Natl Acad Sci U S A. 2005;102:15545–50.
78. Sun XM, Soutar AK. Expression in vitro of alternatively spliced variants of the messenger RNA for human apolipoprotein E receptor-2 identified in human tissues by ribonuclease protection assays. Eur J Biochem. 1999;262:230–9.
79. Sun J, Zhu G, Liu Y, Standley S, Ji A, Tunuguntla R, Wang Y, Claus C, Luo Y, Baudry M, et al. UBE3A Regulates Synaptic Plasticity and Learning and Memory by Controlling SK2 Channel Endocytosis. Cell Rep. 2015;12:449–61.
80. Takahashi H, Katayama K, Sohya K, Miyamoto H, Prasad T, Matsumoto Y, Ota M, Yasuda H, Tsumoto T, Aruga J, et al. Selective control of inhibitory synapse development by Slitrk3-PTPdelta trans-synaptic interaction. Nat Neurosci. 2012;15(389–398):S381–382.
81. Telese F, Ma Q, Perez PM, Notani D, Oh S, Li W, Comoletti D, Ohgi KA, Taylor H, Rosenfeld MG. LRP8-Reelin-Regulated Neuronal Enhancer Signature Underlying Learning and Memory Formation. Neuron. 2015;86:696–710.
82. Trommsdorff M, Gotthardt M, Hiesberger T, Shelton J, Stockinger W, Nimpf J, Hammer RE, Richardson JA, Herz J. Reeler/Disabled-like disruption of neuronal migration in knockout mice lacking the VLDL receptor and ApoE receptor 2. Cell. 1999;97(6):689–701. https://doi.org/10.1016/s0092-8674(00)80782-5.
83. Valente P, Casagrande S, Nieus T, Verstegen AM, Valtorta F, Benfenati F, Baldelli P. Site-specific synapsin I phosphorylation participates in the expression of post-tetanic potentiation and its enhancement by BDNF. J Neurosci. 2012;32(17):5868–79.
84. Wasser CR, Herz J. Splicing therapeutics for Alzheimer's disease. EMBO Mol Med. 2016;8:308–10. https://doi.org/10.15252/emmm.201506067.
85. Wasser CR, Herz J. Reelin: Neurodevelopmental Architect and Homeostatic Regulator of Excitatory Synapses. J Biol Chem. 2017;292:1330–8.
86. Wasser CR, Masiulis I, Durakoglugil MS, Lane-Donovan C, Xian X, Beffert U, Agarwala A, Hammer RE, Herz J. Differential splicing and glycosylation of Apoer2 alters synaptic plasticity and fear learning. Sci Signal. 7;353:ra113.
87. Wightman DP, Jansen IE, Savage JE, Shadrin AA, Bahrami S, Holland D, Rongve A, Borte S, Winsvold BS, Drange OK, et al. A genome-wide association study with 1,126,563 individuals identifies new risk loci for Alzheimer's disease. Nat Genet. 2021;53:1276–82.
88. Yamanaka H, Kamimura K, Tanahashi H, Takahashi K, Asada T, Tabira T. Genetic risk factors in Japanese Alzheimer's disease patients: alpha1-ACT, VLDLR, and ApoE. Neurobiol Aging. 1998;19:S43–46.
89. Yim YS, Kwon Y, Nam J, Yoon HI, Lee K, Kim DG, Kim E, Kim CH, Ko J. Slitrks control excitatory and inhibitory synapse formation with LAR receptor protein tyrosine phosphatases. Proc Natl Acad Sci U S A. 2013;110:4057–62.
90. Yuan R, Li Y, Fu Y, Ning A, Wang D, Zhang R, Yu S, Xu Q. TNIK influence the effects of antipsychotics on Wnt/beta-catenin signaling pathway. Psychopharmacology (Berl). 2021;238(11):3283–92.
91. Zheng H, Koo EH. The amyloid precursor protein: beyond amyloid. Mol Neurodegener. 2006;1:5.
92. Zhou Y, Zhou B, Pache L, Chang M, Khodabakhshi AH, Tanaseichuk O, Benner C, Chanda SK. Metascape provides a biologist-oriented resource for the analysis of systems-level datasets. Nat Commun. 2019;10:1523.
93. Zurhove K, Nakajima C, Herz J, Bock HH, May P. Gamma-secretase limits the inflammatory response through the processing of LRP1. Science signaling. 2008;1(47):ra15. https://doi.org/10.1126/scisignal.116426.

Publisher's Note